U.S. DEPARTMENT OF COMMERCE
NATIONAL OCEANIC AND ATMOSPHERIC ADMINISTRATION
NATIONAL WEATHER SERVICE
NATIONAL METEOROLOGICAL CENTER

OFFICE NOTE 405

BUDGET STUDY OF THE MEAN SHORT RANGE FORECAST ERROR OF THE NMC MRF MODEL

MASAO KANAMITSU
SURANJANA SAHA
DEVELOPMENT DIVISION

JULY 1994

Abstract

A complete budget of the NMC global model forecast systematic error was performed. The budget calculations were directly coded into the operational forecast model, and the systematic errors of the temperature, winds and moisture were diagnosed using 90 N.H. summer cases and 60 winter cases of 1990. The model was integrated for 24 hours and budget calculations were performed at the model sigma levels every time step and accumulated.

One of the important but disappointing results is that this method cannot provide the exact cause of the error. The reason is that there is strong interaction between various terms in the budget equations, particularly between physical processes and the dynamics, and therefore the pattern of one term does not match that of the systematic error. Because of this, the detection of the cause of the systematic error requires highly subjective judgment. Despite this weakness of the approach, this study provided many very useful hints for the improvement of the model. Examples of the problems detected include imbalance between radiative cooling and sensible heating near the land surface, imbalance between radiative cooling and adiabatic warming in the middle troposphere in subtropics and false model response to localized heating due to insufficient horizontal resolution. Based on this study, many of these problems are corrected and the systematic errors of the NMC MRF model were significantly reduced.

1. INTRODUCTION

The finding that systematic errors of models used in major meteorological centers have similarities in pattern and location (Bengtsson and Lange, 1981) has triggered numerous studies (for example, Bettge, 1983 ; Arpe and Klinker, 1986 ; Sumi and Kanamitsu, 1984 ; Klinker and Capaldo, 1986 and others). The development of a gravity wave drag scheme that is aimed at reducing a common westerly bias (Palmer et al., 1986) and the use of an enhanced orography to reduce systematic errors in short term predictions (Wallace et al., 1983) are some of the major developments resulting from such studies. Although these developments and additional improvements in model physics and analysis systems have significantly reduced the magnitude of the systematic errors, these errors still remain as one of the major hurdles in extending the skill of Numerical Weather Prediction (NWP) models beyond one week.

One way to study the systematic error is to design a diagnostic system closely connected to the model dynamics and physics that has immediate application to the improvement of forecast models. This can be accomplished by making complete diagnostics of all the physics as well as the dynamics in the prediction model itself. Such diagnostics have not been commonly performed in the past due to large computational requirements, which are difficult to meet in any operational center because computers are usually used to their full capacity to produce timely forecasts. The first attempt at using diagnostics in the operational model was carried out by Klinker and Sardeshmukh (1988) who examined the systematic errors of the European Center for Medium Range Weather Forecasts model. They performed a large number of one-timestep integrations and recorded separately the contributions of each

individual physical process in the model. This one timestep approach is convenient in reducing the computational overhead. The major assumption in that study is that the error in one-timestep is representative of the error in a short range (e.g. 24-hour) forecast. They compared the distribution and magnitude of the case-averaged contribution of each physical process in the forecast equations with those of the systematic errors. By qualitatively examining the resemblances among the two, they were able to infer several possible problems with their model physics.

Although monitoring of physical processes provides very useful information,, an examination of the contribution of each individual physical process is, in general, not sufficient to construct the total picture of the systematic errors since model dynamics responds to the physical forcings and there is a strong feedback between physics and dynamics and among the physical processes themselves.

In this study, an attempt is made to analyze the forecast error based on the full model equations including the contribution from the dynamics. We examined the geographical pattern, relative magnitude, and sign of all the terms in the prediction equations, including both dynamics and physical processes, averaged over a prediction period and over a large number of cases. Since the average of local time tendencies computed for a large number of samples is very close to zero, any non-zero time-averaged local time tendencies represent the systematic errors of the model. Thus, the budget computation of the forecast equations partitions the systematic error into its various components, whose physical meaning can be identified.

Compared to the study by Klinker and Sardeshmukh (1988), this study is different in the

following respects:

1. Contributions from the dynamics terms were identified and diagnosed. This diagnostic not only completes the budget equation but also provides some insight into the problems due to the dynamics, if they are significant.

2. The model was integrated 24 hours, instead of one timestep. This integration time was based on a limited study of the comparison with the one timestep approach and intended for several purposes; one is to eliminate excessively large tendencies due to any problems in the analysis that result in short time scale spin-up/spin-down. Furthermore, a 24-hour integration makes the contribution to the tendency due to initial adjustment small in the averaging process and avoids the influence of diurnal changes. The one timestep approach is inferior to the 24-hour integration in all these aspects. Secondly, a 24-hour integration is appropriate for studying the systematic error because these errors remain similar in character for forecasts up to about 5 days.

3. Elsewhere we have computed the tendencies of the amplitude of the spherical coefficients of model dependent variables in addition to the tendencies of the variables themselves. This diagnostic provides the energy budget of the total forecast error in total wave number space. This part of the study can be found in Kanamitsu and Saha (1994).

2. FORMULATION, MODEL AND DATA USED

The budget computations were coded directly into a model that was identical to the operational global spectral model (1990). The model had a horizontal resolution of triangular 80 truncation with 18 levels in the vertical. The model physics included long and short wave

radiation with diurnal variation, cloud-radiation interaction, planetary boundary layer processes, deep and shallow convection, large scale condensation, gravity wave drag, enhanced orography, simple hydrology, and vertical and horizontal diffusion. Some details of the model are described in Kanamitsu (1989), and a more complete description is available from NMC Development Division (1988). The analysis scheme used in 1990 was the conventional optimum interpolation scheme described by Dey and Morone (1982). The analysis variables were geopotential height, wind and relative humidity.

In order to obtain an comprehensive depiction of the systematic error, all the prediction equations were taken into consideration in a manner exactly consistent with the model's numerical scheme. In order to accomplish this consistency, care had to be exercised in the evaluation of the linear dynamics terms that are treated semi-implicitly in the model time integration. The linear terms in the divergence and virtual temperature equations, whose values do not appear explicitly were evaluated using the $t+\Delta t$ values obtained after the semi-implicit integration was completed. The correctness of computations was checked to insure that the sum of the terms in the budget calculation equaled the model-computed time tendency without diagnostics.

The equations under consideration were the vorticity, divergence, virtual temperature, and moisture equations, each of which was separated into 12, 5, 13 and 11 terms, respectively. The mass continuity equation was also diagnosed, but the results were rather uninteresting and will not be discussed here. The separation of terms in each of the budget equations studied is described below :

Vorticity equation:

$$\underset{12}{\frac{\partial \zeta}{\partial t}} = \underset{1}{-\vec{V}_\psi \cdot \nabla \zeta} \underset{2}{-\vec{V}_\chi \cdot \nabla \zeta} \underset{3}{-\beta v} \underset{4}{-\zeta D} \underset{5}{-fD} \underset{6}{-\vec{k} \cdot \nabla \times [RT' \nabla \ln p_s]} \underset{7}{+\dot{\sigma} \frac{\partial \vec{V}}{\partial \sigma}} \underset{8}{-F_1} \underset{9}{-F_2} \underset{10}{-F_3} \qquad (1)$$

1. Advection of vorticity by the rotational wind

2. Advection of vorticity by the divergent wind

3. Beta term

4. Relative vorticity stretching

5. Earth vorticity stretching

6. Surface pressure term

7. Vertical advection plus tilting

8. Vertical diffusion

9. Horizontal diffusion

10. Gravity wave drag

11. Difference of implicit and explicit zonal advection

12. Local time tendency (Sum of the above 11 terms)

Note that the NMC model uses implicit zonal advection (Simmons and Jarraud, 1983). The difference between implicit and explicit advection, which does not appear in Eqn. 1, was also monitored in this study (term 11).

Divergence equation:

$$\underset{5}{\frac{\partial D}{\partial t}} = \underset{1}{-\vec{v}\cdot\nabla D} + \underset{1}{\vec{k}\cdot\nabla\times(\zeta+f)\vec{v}} - \nabla^2\left[\underset{1}{\Phi} + \underset{1}{R\bar{T}\pi} + \underset{1}{\frac{\vec{v}\cdot\vec{v}}{2}}\right] - \nabla\cdot\left[\underset{1}{RT'\nabla\pi} + \underset{1}{\dot{\sigma}\frac{\partial\vec{v}}{\partial\sigma}} + \underset{2}{F_1} + \underset{3}{F_2} + \underset{4}{F_3}\right] \qquad (2)$$

1. Dynamics terms
2. Vertical diffusion
3. Horizontal diffusion
4. Gravity wave drag
5. Local time change (sum of the terms 1-4)

The dynamics terms (term 1) are separately computed in the budget calculations but are summed in this study. This is because these terms tend to cancel each other. Furthermore, they are hard to interpret in physically meaningful way for the budget study of the forecast error.

Virtual Temperature Equation

$$\underset{13}{\frac{\partial T_V}{\partial t}} = \underset{1}{-\vec{v}_\psi\cdot\nabla T_V} \underset{2}{-\vec{v}_\chi\cdot\nabla T_V} \underset{3}{-\dot{\sigma}\sigma^\kappa\frac{\partial T_V\sigma^\kappa}{\partial\sigma}} + \underset{4}{\kappa T_V\left(\frac{\partial \ln p_s}{\partial t} + \vec{v}\cdot\nabla\ln p_s\right)} + \underset{5}{F_1} + \underset{6}{F_2} + \underset{7}{F_3} + \underset{8}{F_4} + \underset{9}{F_5} + \underset{10}{F_6} + \underset{11}{F_7} + \underset{12}{F_8} \qquad (3)$$

1. Horizontal advection by the rotational wind
2. Horizontal advection by the divergent wind

3. Vertical advection-like term
4. Surface pressure term
5. Vertical diffusion
6. Horizontal diffusion
7. Convection
8. Large-scale heating
9. Shallow convection
10. Short wave radiation
11. Long wave radiation
12. Change due to moisture change by physics
13. Local time change (sum of the terms 1-12)

The term 12 appears in the equation because the equation is written for virtual temperature, which changes due to the increase or decrease of moisture by various physical processes. In this study, no attempt is made to further partition this change in moisture into various components.

Moisture equation:

$$\underset{11}{\frac{\partial q}{\partial t}} = \underset{1}{-\vec{v}_\psi \cdot \nabla q} \underset{2}{-\vec{v}_\chi \cdot \nabla q} \underset{3}{-\dot{\sigma}\frac{\partial q}{\partial \sigma}} \underset{4}{+Q_1} \underset{5}{+Q_2} \underset{6}{+Q_3} \underset{7}{+Q_4} \underset{8}{+Q_5} \qquad (4)$$

1. Horizontal advection by the rotational wind

2. Horizontal advection by the divergent wind
3. Vertical advection
4. Vertical diffusion
5. Horizontal diffusion
6. Convection
7. Large scale condensation
8. Shallow convection
9. Moisture filling
10. Difference of implicit and explicit zonal advection
11. Local time change (sum of the terms 1-10)

The terms 9 and 10 are related to the numerical techniques and procedures used in the model and do not appear in the original equations but are monitored for completeness.

The partitioning of the horizontal advection term into rotational and divergent parts may require some comments. Because of the terrain-following nature of the sigma coordinate, the divergent part of the wind has a different meaning from that computed on constant pressure surfaces. Despite this difference, it is meaningful to decompose the wind into its divergent and rotational part because the divergent part of the wind is directly related to the physical forcings on the model sigma surfaces including the effect of orography. As will be shown later, the advection by the divergent part of the wind tends to be compensated by the surface pressure term over steep orographic areas.

Since the above budget equations are constructed such that they are strictly consistent

with the model forecast equations, some dynamic terms are in a form that is not very useful to look at. For example, the term that corresponds to the energy conversion from available potential energy to kinetic energy in the thermodynamic equation is imbedded in the vertical advection-like term and the surface pressure term (terms 3 and 4 in Eqn. 3) so that it does not appear explicitly in the forecast equations. The analytical relation may be found from the following expression of the vertical advection-like term:

$$\dot{\sigma}\sigma^{\kappa}\frac{\partial(T\sigma^{-\kappa})}{\partial\sigma}=\dot{\sigma}\frac{\partial T}{\partial\sigma}-\dot{\sigma}\frac{\kappa T}{\sigma} \qquad (5)$$

The first term on the right hand side is the vertical advection of temperature. It is easily shown that the sum of the second term on the right hand side and the surface pressure term (term 4) in Eqn. 3 is the conversion term $\omega\alpha/C_p$. The staggering of the variables used in the NMC model is of the Lorenz type (1960) in which all the dependent variables are defined at model layers while the vertical motion is defined at model interfaces. Because of this staggering, the left hand side of Eqn 5 must be evaluated on the model layers and a vertical averaging is done insuring the energy conservation (Arakawa, 1972). In evaluating the right side of the Eqn. 5, the first term involves the computation of $\delta T/\delta\sigma$, and the second term requires computation of vertical motion, both at the model layers. Such calculation does not appear in the prediction model and therefore, the finite difference form of the right hand side of Eqn. 5 cannot be computed consistently with the model formulation and complete consistency with the forecast model equation will be lost.

It should also be noted that the vorticity and divergence budget expressed in terms of spherical coefficients may easily be converted to a rotational and divergent wind momentum

budget, respectively, by application of a simple inverse Laplacian and space derivative operators in spectral space. The operator to obtain momentum budget from vorticity and divergence may be written as:

$$\frac{\partial \vec{v}_n^m}{\partial t} = -\vec{k}\times\nabla(\nabla^{-2}\zeta_n^m) + \nabla(\nabla^{-2}D_n^m) \qquad (6)$$

It is emphasized that the computation of the budget is performed on the model sigma levels. Care must be exercised in interpreting and comparing the results with other studies using data on constant pressure levels.

In the current study, 92 summer cases (JJA, 1990) and 59 winter cases (JF, 1990), were run with the operational model configuration. This rather large number of cases is essential for studying the systematic error. The model was integrated 24 hours and all the budget terms were computed every time step (Δt=15 min) and accumulated for the period of integration.

3. METHODOLOGY

The cause of the systematic error can most easily be identified if the pattern and the magnitude of the error are identical to those of one of the terms in the budget equation. In most cases, however, it is rather difficult to find a term in the equation which yields a pattern that even roughly resembles that of the systematic error. There are two difficulties involved in identifying the term responsible: The first is a compensation of two large terms, in which case

the pattern of each term does not resemble the pattern of the difference between the two terms. Moreover, even in the case in which the difference field resembles that of the systematic error, it is difficult to judge whether one term is too large or the compensating term is too small. The second is that the leading cause of the systematic error varies from one location to the other. Because of these difficulties, the identification of the processes responsible for the systematic error requires subjective evaluation.

In addition to matching patterns with that of the systematic error, a close examination of the geographical pattern of a term in the budget equation itself can occasionally display potential problems occurring in the model physics, dynamics or analysis. In practice, identification of this type of error can be accomplished without budget calculations. We will treat these errors separately and discuss them in the last part of this paper (Section 5).

Since the volume of output from the diagnostics is extremely large, we had to design some procedure to systematically search for the sources of the systematic errors. In this study, we followed the procedure described below:

(1) Identify latitudes and levels where forecast errors are large in the zonally averaged vertical cross section maps. Then find terms with magnitude similar to or larger than the systematic error over these latitudes and levels.

(2) Examine the geographical distribution of these terms over the selected latitudes and level.

(3) Combine some terms if they are much larger than the systematic error, particularly when they are compensating each other.

(4) Look for the patterns that match the systematic error in these geographical maps.

On many occasions, it is necessary to go back and repeat the procedure from the beginning to refine and confirm the findings.

In identifying the sources of the error, we assumed the degree of inaccuracy of the terms in the budget equation to be in the following order; 1) terms related to the physical processes; 2) dynamics terms related to the divergence and 3) terms related to the rotational wind component. We then assumed that less accurate terms are more likely to be responsible for the error. We realize that the physical basis for this ordering is not very strong since the interactions among all those terms are not negligible. One method to remove this weak point would be to make sensitivity experiments by modifying the terms in question. However, such experiments are nothing less than complete research into the physical processes under consideration and would require more experiments than are practically possible.

It is important to note that the systematic forecast error may result from the error in the analysis. This error can be found from the budget study only if some of the budget terms compensate the error. Such error may be expected to occur over areas where data are known to have some bias or the analysis may not work properly. The error can be detected by looking into the data and changes made to the forecast guess by the analysis (analysis increments). However, in this study, no effort was made to study the analysis component and therefore no firm conclusions are possible for the analysis problems (except for the one presented in Section 5.2). However, we try to mention the possibility of analysis problems whenever the potential is large.

In the following, we will demonstrate the procedure, using the Northern Hemisphere

summer temperature field as an example.

Fig. 2a presents a zonally averaged cross section of the virtual temperature forecast error obtained by averaging 3 months of 24-hour accumulated time tendencies, in units of $x10^{-5}$ degrees per second. Note that the vertical coordinates are model sigma levels, and because of the higher vertical resolution in the lower levels, the spacing of the levels near the ground is greatly exaggerated (see Fig. 1 for the model level configuration). The error patterns are very similar to the 5 day systematic forecast error patterns compiled separately (not shown). The most prominent error in the model during the summer is a positive (warm) error below level 6 (about 850 hPa) in the latitude belt 45°N to 70°N. Although there are several other large negative and positive errors in the cross section map, we will concentrate on this error in this section. Fig. 2b-2k show the budget of all the terms in the thermodynamic equation. Since contributions from horizontal diffusion and moisture terms (terms 6 and 12 of Eq. 3) are negligible, they are excluded from the figures. In order to make the comparison of each term in the thermodynamic equation with the systematic error pattern easy, the contour interval of $0.5x10^{-5}$ K/sec (approximately 0.5 K per day) is used throughout and the zero contour lines are removed.

We will first discuss general features of the budget of heat obtained. Comparing the dynamics terms in the equation, the advection by the rotational part of the wind (Fig. 2b), the vertical advection-like term (Fig. 2e) and the surface pressure term (Fig. 2d) are large compared to most of the other terms. The advection by the divergent part of the wind (Fig. 2c) is large at lower levels, indicating a response to orographic forcings. The surface pressure term (Fig. 2d) is large where high orography is present (around 25N-45N and 70S-90S).

Other dynamics terms also are responding to the surface pressure term over those areas. This is a result of the use of the terrain-following sigma coordinate. There is a poleward transport of heat at around 30S by the advection due to rotational winds. This represents the transport of heat by transient disturbances in the southern hemisphere winter where baroclinic disturbances are active. The vertical advection-like term (Fig. 2e, note the comment in the previous section, Eq. 5) shows adiabatic cooling associated with upward motion caused by the convective heating in the tropics (Fig. 2f) and adiabatic warming due to descending motion of the Hadley circulation in the subtropics. Among the physics terms, the vertical diffusion term (Fig. 2k) is the largest and is concentrated in the boundary layer. The convective heating (Fig. 2f) has a maximum at around 5N with magnitude of about $3x10^{-5}$ K/sec at level 10 (around 500 hPa) and secondary maxima located at around 40S at level 5 (around 850 hPa). The maximum of the large scale condensation (Fig. 2g) is located in the southern hemisphere high latitude storm tracks. The contribution of the shallow convection is not negligible. Its maxima are located in the subtropical and tropical lower troposphere. These figures show that this budget of forecast error is also useful as a budget study of the general circulation of the global atmosphere, and the results obtained in this study are meteorologically quite reasonable. That aspect of using this budget calculation for the observational study is under preparation.

Turning back to the systematic error: For the warming error over 45°N-70°N at level 1, the error is affected significantly by a large positive contribution from vertical diffusion (Fig. 2k), a negative contribution from horizontal advection by the divergent part of the wind (Fig.

2c), a negative contribution by the surface pressure term (Fig. 2d), and a negative contribution by the longwave heating (Fig. 2i). Note that at these low levels, the effect of the advection-like term (dry adiabatic cooling) is small (Fig. 2e). The contributions from the dynamics terms have smaller north-south scales than the systematic error (Fig. 2a). Such difference in the meridional scale is not observed in the physics terms. Since the systematic error is a summation of the dynamics and the physics terms, this difference in scale in the dynamics terms indicates that cancellation must be taking place among the dynamics terms.

Based on these observations, we next examine the geographical distribution of the large terms noted above. A geographical map of virtual temperature tendency at level 1 over the area 45N to 75N was examined and large positive errors were found over North America, Russia and China. Fig. 3a shows the systematic error over the Eurasian continent portion of this latitudinal band: it is up to +3 K and covers the entire continent (contour interval is 0.5×10^{-5} $Ksec^{-1}$). The horizontal advection by the rotational wind (Fig. 3b), by the divergent wind (Fig. 3c), the surface pressure term (Fig. 3d) and the vertical diffusion term (Fig. 3e) are all nearly 4 times greater in magnitude than the systematic model tendency (contour interval is 2.0×10^{-5} $Ksec^{-1}$). The sum of these terms shown in Fig. 3f (contour interval is 0.5×10^{-5} $Ksec^{-1}$) does not resemble the systematic error. The magnitude is larger than the systematic error and its horizontal scale is smaller. After searching through the other terms, we discovered that the horizontal diffusion term (Fig. 3g), which is very small in the zonal average field, has small scale features that compensates the small scale peaks in the summation. This is an example of how tendencies that are small in the zonal average, may make a significant contribution to the local geographical distributions and the procedure

presented in the beginning of this section need to be revised in some cases. The sum of Fig. 3f and 3g is presented in Fig. 3h. The large scale pattern of Fig. 3h somewhat resembles that of the systematic error, but there are some differences in detail. Since Fig. 3h is a summation of many terms, this resemblance cannot reveal which of the terms is the source of the systematic error. We next examined the contribution of longwave warming (Fig. 3i). We found patterns surprisingly similar to the systematic error over several locations (note the pattern at around 70N, 80E and an area centering 63N, 110E). This suggests too little radiative cooling over the continent, pointing to a possible problem in the treatment of long wave radiation near the surface in the NMC global model. There is some concern regarding the choice of the model temperature to be used for the longwave calculation. The model uses surface skin temperature; an alternate choice would be the use of the lowest model air temperature extrapolated to the surface. This aspect of the radiation calculation is under investigation.

4. Results of the budget study

The example in the last section presented the subjective and somewhat elaborate procedures necessary to find the potential causes of the systematic errors. Since it is not practical to present such procedures for all the results obtained in this study, we minimize the description of the procedures and focus on the results. We further avoid describing all the systematic errors appearing in the mean maps and concentrate on the physically meaningful errors that directly relate to model improvements. This approach excludes many of the large amplitude systematic errors that cannot be explained from this budget study. In the following

subsections, systematic errors are classified by their possible physical causes and described.

4.1 Some general remarks on the systematic error

Some of the terms in the budget equation were found to have fairly small scale features. An example is shown in Fig. 3b-Fig 3e. These small scale features tend to be located over orographic areas, and have a property of cancelling out with other terms in the equation, making the systematic error much larger scale. Since we are not interested in such small scale details that do not appear in the systematic error itself, we applied a T40 filter to the budget results in some of the cases presented below (The example in the previous section is not filtered). The filtering is applied after all the computations are made using full T80 coefficients, so that the filtered results contain the effect from scales smaller than T40.

The budget equations used in this study include several terms that are not physically meaningful or significant but exist for numerical reasons. These are: the difference between explicit and implicit zonal advection of vorticity and moisture, moisture filling (avoiding negative specific humidity) and virtual temperature change due to the change in moisture by various physical processes. Some of those terms, for example moisture filling, show some systematic patterns but they are 1-2 orders of magnitude smaller than the systematic error itself. Thus these minor terms are not the cause of the systematic error.

4.2 Errors due to surface exchange and radiation near the surface

The errors due to excessive surface heat exchange and/or weak radiative cooling discussed in the previous section are commonly found at the model's lowest level in both summer and

winter seasons in northern hemisphere dry land areas. Geographically, the errors are located over the Sahel in the northern hemisphere winter (not shown). In the northern hemisphere summer, they are located further north over North America, Russia (discussed in the previous section) and northern China (Fig. 3a). It is noted that the terms related to orography, i.e., the surface pressure term and the advection due to the divergent part of the wind, are not large over these areas, except over the orographic areas along the southern edge of the domain shown.

In addition to the erroneous longwave cooling near the surface discussed in the previous section, there are several possible reasons for the occurrence of the warm error: One is that the systematic warm error resulted from a too-high ground temperature over non-orographic areas. This may be caused by a weakness in solar radiation calculation or in the specification of surface conditions such as albedo and soil wetness. If the problem lies in the short wave radiation, the treatment of clouds may play a role, as well as the exclusion of aerosols, which can be important over the desert areas. It is also noted that the analysis may be at fault, reducing the near-surface temperature at every analysis time. Although the area shown is reasonably well covered by observations, such error in analysis may occur because the analysis variable is height and the temperature is computed from the thickness. Very thin model layers near the surface may introduce unexpected computational problems. In this study, no further examinations of analysis problems are performed.

In the areas with more orographic influence, e.g. over India and southern China in winter (not shown), the contributions of dynamics terms, namely the surface pressure term and the advection by the divergent part of the wind, become large and offset the surface

heating, and therefore, it is not clear which term is causing the error. The errors associated with orography-related terms are also found along the coast of Antarctica (see Figs. 2a-e over Antarctica, 70S-90S).

Aside from the error due to sensible heating and radiation, the area of positive temperature error in the southern hemisphere winter near 55°S-65°S along the coast of Antarctica at model sigma level 1 matched quite closely in pattern that of the vertical diffusion tendency (see shaded areas in Fig. 4a and b). Since the error covers nearly the entire longitude belt, this error is also clearly identified in the zonal average cross section maps (Fig. 2a and 2k). There is some possibility that this error is related not to the physics but to the sea-surface-temperature derived from the satellite observations where the existence of clouds over the "roaring 50s" may contaminate the observation. However, insufficient surface data coverage over the area make it difficult to come to any firm conclusions.

There is some indication that the systematic error related to the surface exchange processes also exists in the moisture field. The error tendency pattern of moisture at level 1 in the Northern Hemisphere winter shows a large positive area over the Sea of Japan, over the ocean to the south of Japan and over southeastern China (see shaded areas in Fig. 5a). The contribution of vertical diffusion tendency (see shaded areas in Fig. 5b) seems to have some similarity in patterns over the Sea of Japan and over the ocean to the south of southern Japan. Because of the large amplitude in the contribution of this term, particularly over the south China sea, the pattern correlation is not very apparent. However, some correlation still exist between the systematic error and the vertical diffusion. These areas are known to produce very large latent heat fluxes. In cases of such extreme evaporation, the model may be

overestimating the latent heat fluxes. For this error also, lack of moisture observations and weakness in the moisture analysis make it difficult to make definite statements.

4.3 Error due to vertical diffusion above the boundary layer

The errors related to vertical diffusion are found mostly in the temperature in the middle troposphere. At these levels, the vertical diffusion has the same sign as the errors themselves, suggesting that the vertical mixing process is excessive. Typical positive errors in temperature of this type were found in a narrow zone near 33°S from the west coast of Australia to east of the dateline at level 10 (about 500 hPa) in the southern hemisphere winter (see shaded areas in Fig. 6a-b). Although small scale details do not agree in the two figures (for example, the peaks appear in the error field over the southwestern tip of Australia), the broad zone of positive error and the contribution of vertical diffusion match fairly well.

The vertical diffusion in the NMC global model uses Richardson number-dependent diffusion coefficients. The diffusion coefficient becomes large where static stability is small or vertical wind shear is large. An examination of the 3-month mean vertical wind shear and the stability over the area did not show typical features that explain the large vertical diffusion (not shown). It is possible that the large vertical diffusion occurred in sporadic manner and did not show up in the mean field. Distribution of the seasonal mean Richardson number may be helpful but was not available for this study.

The vertical diffusion process is primarily based on the observation and theory of the planetary boundary layer and more general application to the free atmosphere may not be appropriate. Moreover, vertical diffusion may be important for numerical reason rather than

for physical reason. As shown in Kanamitsu and Saha (1994), there is a strong interaction between horizontal diffusion and the vertical diffusion indicating that the vertical diffusion is acting as a suppressor of noise generated in the model. These aspects make it very difficult to further improve the vertical diffusion processes. Work is planned to address these questions.

4.4 Error over subsidence area

In the cross section maps of the heat budget, a broad band of warming exists across all latitudes at level 10 (Fig. 15a). Comparison of the sum of the dynamics terms and the sum of the physics terms shows that in the extratropics the cooling by physics is not balanced with the adiabatic warming caused by the descending branch of the Hadley circulation (not shown). A similar diagnosis was made from the geographical distribution of temperature errors at this level. The positive errors in the extra tropics are located over the eastern oceans in the southern (summer) hemisphere, i.e. west coast of South America and the west coast of Africa and south equatorial Atlantic Ocean (see shaded areas in Fig. 7a). In these areas, we find that warming comes from the sum of the dynamics terms (see shaded areas in Fig. 7b). Partitioning of the dynamics terms into vertical motion dependent and independent terms could not reveal clearly the role of the descending motion over the areas, due to the fact that large cancellations among the dynamics terms taking place over the orographic area overshadowed the detailed budget over the ocean. This cancellation is an artifact of computations of the budget on the model sigma surface and is a weak point of this approach.

There are two possible causes for the warm temperature error to occur over these areas.

The first is that the physics, mainly radiation, is not sufficient to offset the diabatic warming (Fig. 7c). Note that since the areas of interest are characterized by descending motion, physical processes other than radiation are not significant. The second possible cause of the warming error is that the excessive convection over the summer hemispheric continents creates excessive subsidence over the adjacent oceans. The static stability over the descending area is also crucial. Since quantitative verification of precipitation over the tropical continents is very difficult, confirmation of this possibility is not easy. However, the general weakening of the Hadley circulation (to be discussed in the next subsection) may exclude the possibility of excessive convection.

Over and near the area of active convection, during the Northern Hemisphere summer, we also observe a positive temperature error (Fig. 8a and b, see shaded areas), over the central Pacific and Indian Ocean. The cooling by longwave radiation shown in Fig. 8c has very little correspondence with the convective heating pattern. Although the convective heating is mostly compensated by the dynamic dry adiabatic cooling, some correspondence with radiation is expected through the radiation-cloudiness interaction. In fact in the NMC model, the convective cloudiness parameterization assumes a pre-specified amount of low/middle/high clouds depending on the precipitation and the height of the convection. In addition, coexistence of convective and stratiform clouds is not allowed. Improvement in the cloudiness parameterization and the cloud property specification is now in progress and will address these questions.

The error over the descending area is also found in the moisture field. Pockets of large negative errors along the west coast of the United States over the Pacific Ocean (Fig. 9a, see

shaded areas), and over Cuba and Latin America in the western Atlantic Basin (not shown) at level 6 are examples. These errors correlate very well with the tendency from the sum of the dynamics terms (see Eqn. 4). Among the three dynamics terms, the tendency due to downward vertical advection of moisture (Fig. 9b) corresponds both in pattern and magnitude with this error, indicating too strong subsidence caused probably by too strong convection nearby or by insufficient vertical eddy transport of moisture (Fig. 9c and 9d).

4.5 Error due to convection

A positive heating error found over the Andes mountains of South America at level 8 in southern hemisphere summer (Fig. 10a) has a good correlation with the pattern of tendency due to the sum of the physics terms, the largest term being that of convective heating (Fig. 10b, compare shaded areas). The magnitude of the convective heating is much larger than the error because the dynamics terms tend offset the convective heating. Based on the assumption described earlier in section 3, excessive convection is the first candidate for the cause of the systematic error. It is well known that models generate excessive convection over these areas. This error is related to the erroneous sensible heating over the steep slope of the Andes mountains and will be discussed in the next section. The problem has been greatly reduced with the increase in horizontal resolution (from T80 to T126) and the use of non-enhanced mean orography in the present operational model.

The effect of convection is also seen in the systematic error of the divergent part of the wind. The large positive errors of divergent wind at level 5 in winter (Fig. 11a, unit in m/sec/sec) are located over the ITCZ active areas along the lower branches of the Hadley circulation. The largest error is in the meridional component except over Africa and South America. Compared to the analyzed divergent wind shown Fig. 11b (note this is a full field of divergent wind and not the error, unit in m/sec), this error represents either a northward shift of the ITCZ in the forecast particularly over the western Pacific, or a weakening of the northerly divergent flow. The divergent wind error over the two continents implies a strengthening of the easterly divergent circulation into the continent. At the level corresponding to the upper branch of the Hadley circulation in the tropics, at around model

level 14, the pattern of error tendency (not shown) is similar but opposite in sign to the pattern of error found at Level 5. An examination of the divergent wind error at this level shows a similar strengthening/weakening process (but opposite in sign) as described earlier.

These errors indicate a strengthening of zonal convergence over the continents. The convergence due to the meridional component of the wind, on the other hand, is weakening in the model forecast. As a total, the Hadley circulation appears to weaken in the model, in support of the study by White (1988).

4.6 Error at or near the top of the model

We observe significant errors at or near the top levels of the model in temperature and wind fields particularly at high latitudes (for example, see Fig. 2a). Major physical processes at these levels are the radiation in the thermodynamic equation and the gravity wave drag in the momentum equations. These physical processes are much smaller than the contribution due to dynamics terms at these levels, except for gravity wave drag over some localized places (over Himalayas, Alaska and Scandinavia) and therefore, most of the errors appear to come from the dynamics terms. The partitioning of the dynamics terms into rotational and divergent related terms normally shows the patterns compensating each other. An example shown in Fig. 12b and 12c clearly demonstrates this property. As a result of this compensation, both divergent and rotational terms do not resemble the forecast error pattern (Fig 12a), and are not responsible for the systematic error. It is very likely that the upper boundary condition distort the vertical motion at the levels close to the top and generates errors. In this case, we expect that the term related to the vertical motion resembles the

systematic error. However, such resemblance was not found, probably due to the strong interaction between the divergence related terms and the rotational wind related term.

5. ERRORS IDENTIFIED BY ERRONEOUS PATTERNS

Some model problems can be found by simply looking for unnatural geographical patterns. This subjective method is useful, particularly when the contribution of erroneous physics in the model is entirely compensated by the dynamics and/or other physics, and no systematic error is associated with it.

5.1 Erroneous sensible heating

Figure 14a shows the geographical distribution of the vertical diffusion tendency at the lowest model sigma level in the thermodynamic equation in the southern hemisphere summer. The effect of the vertical diffusion at this level comes mainly from surface sensible heating. We observe bands of maximum sensible heating along the coastlines of the continents and along the steep slopes of the Andes mountains in South America. A similar area of maximum sensible heating is observed over the steep slopes facing south over the Himalayan ranges during the northern hemisphere summer (not shown). This strong sensible heating over land is compensated by three terms; horizontal advection of cold air from the adjacent oceans (Figure 13b) ; adiabatic cooling due to upslope winds represented by advection due to the divergent wind (Figure 13c) and the surface pressure term over the steep slopes (Figure 13d) . As a result of this cancellation of terms, no systematic error is observed over these regions (note that over flat dry surfaces, such as over South Africa and the Saharan desert during the

northern summer, such a dynamical response is clearly lacking and no strong sensible heating is observed).

Since there is no observational evidence in support of such strong sensible heating over steep mountain slopes and coastal areas, it is likely that its presence in the model forecasts is unrealistic. In reality, the dynamical response to the surface heating in these areas must take place in a localized small-scale circulation, i.e . in the form of a sea-breeze circulation near coastal areas, and mountain/valley circulation over the steep mountain slopes. These local circulations are normally of the order of several kilometers only. Since the global model has a resolution of about 100-200 kilometers (160 Km for T80 resolution), it is not possible to resolve such small-scale dynamic responses in the model. This erroneous dynamical response in the model will not cause serious large-scale errors if the circulation does not interact with other physics, as in the case of the sensible heating maxima along the coasts, where the circulation is limited to shallow layers near the earth's surface. However, the circulation occasionally interacts with cumulus convection and this amplifies the erroneous circulation. This happens over the Andes mountains, where large erroneous convective precipitation is produced in the forecast along the mountain ranges during the southern hemisphere summer.

This problem has been reduced to a great extent in the current operational model, due partly to its higher resolution (T126), as well as to the use of mean orography and other minor improvements. However, weak erroneous precipitation still remains. A fundamental remedy of this recurrent problem must come either from the use of an extremely high resolution model that resolves the local circulations (which is not feasible due to current limitations on computing power), or from the development of a parameterization of local

circulations in coarser resolution models. Unfortunately, no such parameterization has ever been developed (except gravity wave drag).

5.2 Moisture bogus data problem

Another example of error identified by the unnatural patterns was traced back to an error in the data itself. The unnatural shape of a large positive error area is found over the central and eastern Pacific Ocean off the west coast of North America at level 1 (Fig. 14a, see shaded area and east-west oriented isoline marked "A"). A similar pattern was found in the vertical diffusion term (effect of evaporation, see shaded area and the orientation of the isoline marked "B") with the same sign (Fig. 14b). From a budget analysis point of view, this suggests that the evaporation over the area is erroneous. Searching into the moisture data used in the analysis over the area, we discovered that the area covered by moisture bogus data derived from satellite visible images coincided with the systematic error pattern. Further examination revealed that the moisture bogus data were mishandled in the analysis in such a way that the analysis tend to dry out the initial guess fields over the area. After the finding, the handling of the data was corrected and the systematic error in moisture over the area was significantly reduced. When a new analysis system (Parrish and Derber, 1993) was introduced in the summer of 1991, the use of moisture bogus data was discontinued due to the difficulty in assigning a reasonable observational error.

6. CONCLUSIONS

A complete budget of the NMC global model forecast systematic error was performed. The budget calculations were directly coded into the operational forecast model, and the systematic errors of the temperature, winds and moisture were diagnosed using 90 N.H. summer cases and 60 winter cases of 1990. The model was integrated for 24 hours and budget calculations were performed at the model sigma levels every time step and accumulated.

One of the important but disappointing results is that this method cannot provide the exact cause of the error. The reason is that there is strong interaction between various terms in the budget equations, particularly between physical processes and the dynamics, and one term never matches exactly the systematic error. Computing the budget on model sigma surfaces also made the study somewhat more difficult due to additional terms appearing in the equations, that tend to cancel with other terms. Interpretation of advection by rotational and divergent winds also suffered from differences in their physical meaning on the terrain-following sigma surface. Despite these weaknesses, subjective judgment based on the accuracy of the terms in the budget equation provided many very useful hints for the improvement of the model. Some of the problems were already known to us from problems in (or omission of) some of the physical parameterizations in the model. However, the demonstration of how such weaknesses in the physics can create systematic errors in real cases was also very helpful. In the following, typical forecast errors and the associated model problems found in this study are summarized.

6.1 Temperature

Errors near the surface are located over land, and occur in areas where the insolation is large and the sensible heating is largest. Thus the errors tend to locate in northern hemisphere continent. Due to the proximity to the lower boundary condition, adiabatic cooling associated with the vertical motions cannot compensate the heating over the flat areas, so that dynamics terms do not play a role in the budget equation. At this level, the systematic error is due to an imbalance between the sensible heating and the radiative cooling. Errors in the analysis of near-ground temperatures may also contribute to the systematic bias, but this is not easy to demonstrate. Over the orographic areas, the heating is compensated by the divergent circulations along the sloping surfaces. Surface discontinuities, such as coastlines, can also generate a dynamical response through horizontal advection. Over these regions, even though erroneous forcing may exist, it does not appear in the systematic error fields.

Systematic errors at mid tropospheric levels seem to come from two sources : an imbalance between subsidence warming and radiative cooling over subtropical areas, and regions where the vertical diffusion is excessive.

At upper levels, particularly in the stratosphere, the systematic error is mainly due to errors in tendencies of the dynamics terms, for the effect of the physics terms is very small. The effect of the top boundary condition on the systematic error could not be demonstrated properly in this budget study.

6.2 Rotational wind

There is some indication that inadequate vertical resolution and staggering of variables in the vertical is related to the systematic errors in the subtropics in the upper troposphere. In the model, all the dependent variables are defined at the model layers while vertical motion is defined at the interfaces. For the vertical motion related terms, some vertical averaging process is carried out, but this may have the potential of causing vertical displacement in the computed quantities especially where vertical wind shear is large.

At very high levels over high latitudes, gravity wave drag is too strong and contributes to the systematic bias over some localized polar regions in the northern hemisphere stratosphere.

6.3 Divergent winds

The budget of the forecast error in the divergent part of the momentum field is much harder to analyze. This is due to the non-conservative property of divergence fields and to the character of these fields, which basically are the result of the forcings in the model. The forecast error in the strengthening of the divergent circulation over continents and a weakening over oceans in the tropics are major findings. These errors are apparently related to the convective heating over the continents.

6.4 Moisture

An apparent problem in the moisture bogus data was detected from the unnatural pattern of systematic error itself. Due to the difficulties in analyzing moisture because of its inherent small spatial scale, lack of observations, lack of strict physical relationship with other

variables and close connection to physical processes in the model, the budget of the forecast error of the moisture was very hard to interpret.

Since 1990, when the computations in this study were performed, significant progress has been made in global modeling and analysis at NMC. Some of the major upgrades in the operating system include an increase of horizontal resolution to T126, incorporation of marine stratus in the radiation computation, improvement of horizontal diffusion in 1990 (Kanamitsu, et al., 1990), introduction of 3-dimensional variational analysis in 1991 (Parrish and Derber, 1993), increase in vertical resolution from 18 to 28 levels, and introduction of a new mass-flux scheme for convective parameterization by Pan and Wu (1994) in 1993. In Fig. 15a-c, cross sections of the 1-day systematic errors in the temperature fields for the summers of 1990, 1992 and 1993 are presented (note that the contour interval in these figures is 0.25 K and Fig. 2a is reprocessed to produce Fig. 15a). The figures for 1992 and 93 were provided by Dr. Glenn White of NMC. Compared with the systematic errors examined in this study (Fig. 15a), it is very clear that the error was significantly reduced from 1990 to 1992 and from 1992 to 1993. Similar reduction was found in other variables. It is interesting to see that there is a common pattern in the errors for all three years. This may indicate that some of the errors noted in this paper still remain in the model. Budget studies as described in this paper will be performed with the latest operational model to further reduce the systematic error.

ACKNOWLEDGEMENTS

We would like to thank Dr. G. White for carefully reviewing the paper and providing Fig. 15 for this study. We also would like to thank Drs. P. Caplan and J. Gerrity for reviewing the paper and giving us valuable comments. We thank Dr. E. Kalnay for her continuous encouragement in pursuing the work.

REFERENCES

Arpe, K. and E. Klinker, 1986: Systematic errors of the ECMWF operational forecasting model in mid-latitudes. *Quart. J. R. Met. Soc.*, **112**, 181-202.

Arakawa, A., 1972: Design of the UCLA general circulation model. Numerical Simulation of Weather and Climate, Tech. Rep. No. 7, Dept of Meteorologgy, University of California, 116pp.

Bengtsson, L. and A. Lange, 1981: The results of the WMO/CAS NWP Data Study and Intercomparison Project for Forecasts for the Northern Hemisphere in 1979-80. PWPR Report No. 1. Available from WMO, Geneva, Switzerland.

Bettge, T. W., 1983: A new systematic error comparison between the ECMWF and NMC prediction models. *Mon. Wea. Rev.*, **111**, 2385-2389.

Dey, C. H. and L. L. Morone, 1985: Evolution of the National Meteorological Center Global Data Assimilation System: January 1982-December 1983. *Mon. Wea. Rev.*, **113**, 304-318.

Fels, S. B. and M. D. Shwarzkopf, 1975: The simplified exchange approximation - a new method for radiative transfer calculations. *J. Atmos. Sci.*, **32**, 1475-1488.

Kanamitsu, M., 1989: Description of the NMC Global Data Assimilation and Forecast System. Weather and Forecasting, 4, 335-342

_____, J. C. Alpert, K. A. Campana, P. M. Caplan, G. G. Deaven, M. Iredell, B. Katz, H.-L., Pan, J. Sela and G. H. White, 1991: Recent Changes Implemented into the Global Forecast System at NMC. *Wea. Forecasting*, **6**, 425-435.

_____, M. and S. Saha, 1994 : Spectral Energetics Analysis of the short range forecast error of the NMC MRF Model. Submitted to Monthly Weather Review.

Klinker , E. and M. Capaldo, 1986: Systematic errors in the baroclinic waves of the ECMWF model. *Tellus*, **38A**, 215-235.

Klinker, E. and P. D. Sardeshmukh, 1988: The diagnosis of systematic error in numerical weather prediction models. Workshop Proceedings, Diabatic Heating, 30 November - 2, December, 1987. ECMWF.

Lorenz, E., N., 1960: Energy and numerical weather prediction. *Tellus*, **12**, 364-373.

NMC Development Division, 1988: *Documentation of the Research Version of the NMC Medium Range Forecasting Model.* Available from NMC Development Division, W/NMC2, WWB, Washington, D.C. 20233.

Palmer, T. N., G. J. Shutts and R. Swinbank, 1986: Alleviation of a systematic westerly bias in general circulation and numerical weather prediction models through an orographic gravity wave drag parameterization. *Quart. J. R. Met. Soc.*, **112**, 1001-1039.

Pan, Hua-Lu and Wan-Shu Wu, 1994: Implementing a Mass Flux Convection Parameterization Package for the NMC Medium-Range Forecast Model.
To be submitted to Mon. Wea. Rev.

Simmons, A. J. and M. Jarraud, 1983: The design and performance of the new ECMWF operational model, in *ECMWF Workshop on Numerical Methods for Weather Prediction*, Vol 2, 5-9 September 1983, 113-164.

Sumi. A. and M. Kanamitsu, 1984: A study of systematic erorrs in a numerical prediction model, Part I: General aspects of the systematic errors and their relation with the transient eddies. *J. Met. Soc. Japan,* **62**, 234-251.

Wallace, J. M., S. Tibaldi and A. J. Simmons, 1983: Reduction of systematic forecast errors in the ECMWF model through the introduction of an envelope orography. *Quart. J. R. Met. Soc.*, **109**, 683-717.

White, G. H., 1988: The MRF Model: Systematic errors in medium and extended range forecasts. Workshop on Systematic Errors in Models of the Atmosphere, Toronto, Canada, World Meteorological Organization.

FIGURE LEGEND

Figure 1. Model vertical structure. Model layers displayed are where all the dependent variables are defined. Model layer interfaces are not shown but the lowest level is at the surface (sigma=1) and the top is at sigma=0.

Figure 2a. Mean zonally averaged virtual temperature budget for June-July-August 1990 as a function of model sigma levels, in units of 10^{-5} K/sec. Contour interval is 0.5×10^{-5} K/sec. Contribution by a) Local time tendency (i.e. systematic error), b) Horizontal advection by rotational wind, c) Horizontal advection by divergent wind, d) Surface pressure term, e) Vertical advection-like term, f) Convection, g) Large-scale heating, h) Shallow convection, i) Longwave radiation, j) Shortwave radiation, k) Vertical diffusion.

Figure 3. Mean virtual temperature budget, averaged for June-July-August 1990, at model sigma level 1 (about 995 hPa) for the area 0°-180°E and 45°N-75°N (Europe and Russia), in units of 10^{-5} K/sec, for a) Local time tendency (systematic error), b) Advection by the rotational part of the winds, c) Advection by the divergent part of the wind, d) Surface pressure term, e) Vertical diffusion, f) Sum of b), c), d) and e), g) Horizontal diffusion, h) Sum of all the terms except long wave radiation, i) Long wave radiation. Contour interval is 0.5×10^{-5} K/sec for a), f), g), h), i) and 2.0×10^{-5} K/sec for b), c), d), e).

Figure 4. (a) Systematic error of temperature at model level 1 (about 995 hPa) for June-July-August 1990 in the southern hemisphere, and (b) contribution of vertical diffusion to the systematic error. Units in K/sec, contour intervals are 0.5×10^{-5} K/sec for a) and 5×10^{-5} for b).

Figure 5. a) Systematic error of moisture averaged for Jan.-Feb. 1990 at model sigma level 1 (about 998 hPa) for the far east. b) Contribution of vertical diffusion to the moisture error budget over the same area. The fields are filtered by taking T40 portion of the T80 coefficients. Unit in 10^{-8} Kg/Kg/sec., contour interval 0.5×10^{-8} Kg/Kg/sec.

Figure 6. (a) Systematic error of temperature averaged for June-July-August 1990 at model level 10 (about 424 hPa) over Australian area and (b) contribution of vertical diffusion to the systematic error. The fields are filtered by taking T40 portion of the T80 coefficients. Units in K/sec and contour interval 3×10^{-5} K/sec.

Figure 7. (a) Systematic error of temperature averaged for June-July-August 1990 at model level 10 (about 424 hPa) over the area covering south America and Africa, (b) contribution of dynamics terms to the systematic error and (c) contribution by the longwave heating. The fields are filtered by taking T40 portion of the T80 coefficients. Units in K/sec and contour interval 0.3×10^{-5} K/sec for (a), 1.0×10^{-5} K/sec for (b) and 0.2×10^{-5} K/sec for (c).

Figure 8. (a) Systematic error of temperature averaged for June-July-August 1990 at model level 10 (about 424 hPa) over the equatorial western Pacific, (b) Contribution of convection to

the error and (c) contribution of the longwave heating. The fields are filtered by taking T40 portion of the T80 coefficients. Units in K/sec and contour interval 0.3×10^{-5} K/sec for (a), 1.0×10^{-5} K/sec for (b) and 0.1×10^{-5} K/sec for (c).

Figure 9. (a) Systematic error of specific humidity for January-February 1990 at model level 5 (about 856 hPa) over the eastern equatorial Pacific, (b) contributions of advection by divergent part of the wind and vertical advection to the systematic error. The fields are filtered by taking T40 portion of the T80 coefficients. Unit in Kg/Kg/sec., contour interval 0.5×10^{-8} Kg/Kg/sec.

Figure 10. (a) Systematic error of temperature averaged for January-February 1990 at model level 8 (about 593 hPa) over South America and (b) contribution of convective heating to the systematic error. The fields are filtered by taking T40 portion of the T80 coefficients. Units in K/sec and contour interval 0.2×10^{-5} K/sec for (a), 1.0×10^{-5} K/sec for (b).

Figure 11. (a) Systematic error of the divergent component of the wind over the tropical belt averaged for January-February 1990. Unit in m/sec/sec. (b) Mean divergent wind vector over the same area. Unit in m/sec.

Figure 12. (a) Systematic error of temperature at the model level 17 (about 74 hPa) over the northern hemisphere high latitudes averaged for January-February 1990, (b) contribution of the advection of temperature by the rotational part of the wind and (c) contribution of the sum

of the advection by the divergent winds, surface pressure term and the vertical advection-like term. All the fields are filtered by taking T10 portion of the T80 spectral coefficients. Units in K/sec and contour interval 1.0×10^{-5} K/sec for (a), 3.0×10^{-5} K/sec for (b) and (c).

Figure 13. Contribution of various terms of the heat budget at model level 1 (about 995 hPa) over the selected southern hemisphere zone. Contribution of (a) vertical diffusion, (b) advection by the rotational part of the wind, (c) advection by the divergent part of the wind and (d) surface pressure term. Unit in 10^{-5} K/sec.

Figure 14. Mean moisture, averaged for Jan-Feb 1990, at model sigma level 1 for the area 180°W-90°W and Eq-60°N (Pacific and west coast of U.S.) , in units of 10^{-8} Kg/Kg/second for: a) Local time tendency and b) Contribution to the local time tendency from the vertical diffusion term.

Figure 15. Comparison of the zonally averaged day-1 temperature forecast error for June-July-August of (a) 1990, (b) 1992 and (c) 1993. Contour interval is 0.25K. (a) is produced by reprocessing Fig. 2a, converting tendency to day-1 temperature error and using 0.25K contour interval. Note that the vertical scale of (a) is different from that of (b) and (c).

Layer #	Thickness	Pressure	Mandatory levels
			20
18	0.050	21mb	30
			50
17	0.050	74	
			100
16	0.050	124	
			150
15	0.050	175	
			200
14	0.050	225	
			250
13	0.050	295	
			300
12	0.050	325	
11	0.050	375	
			400
10	0.050	425	
9	0.096	497	500
8	0.096	594	
7	0.093	688	
			700
6	0.085	777	
5	0.073	855	
			850
4	0.055	920	
3	0.025	960	
2	0.017	961	
1	0.010	995	1000

Fig 1

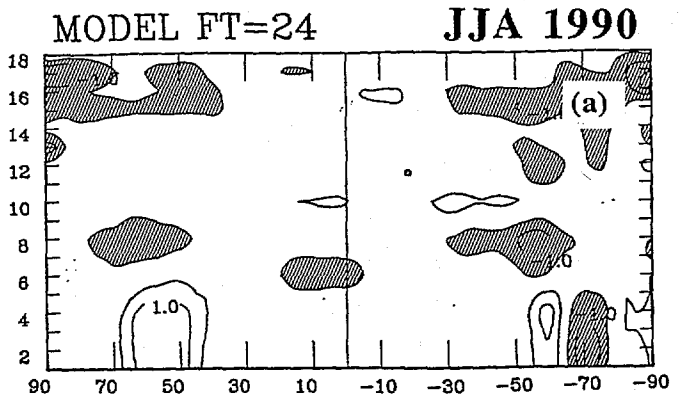
MODEL FT=24
JJA 1990
(a)
18
16
14
12
10
8
6
4
2
90 70 50 30 10 -10 -30 -50 -70 -90

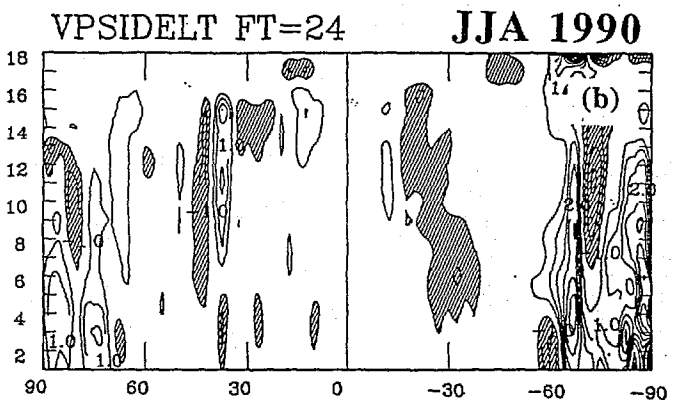
VPSIDELT FT=24
JJA 1990
(b)
18
16
14
12
10
8
6
4
2
90 60 30 0 -30 -60 -90

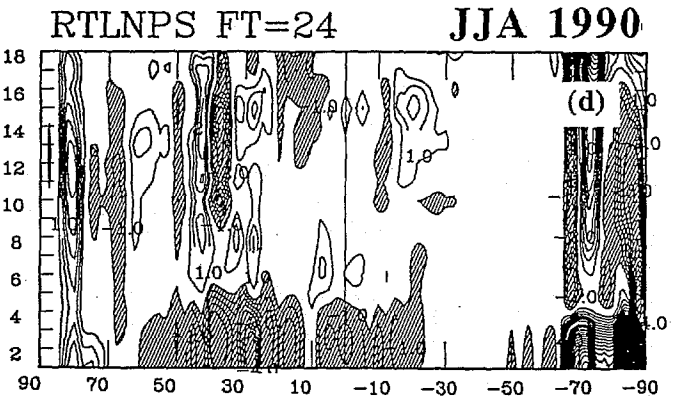
RTLNPS FT=24
JJA 1990
(d)
18
16
14
12
10
8
6
4
2
90 70 50 30 10 -10 -30 -50 -70 -90

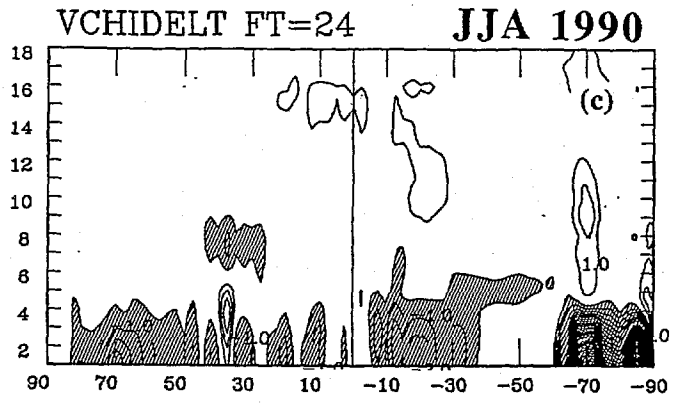
VCHIDELT FT=24
JJA 1990
(c)
18
16
14
12
10
8
6
4
2
90 70 50 30 10 -10 -30 -50 -70 -90

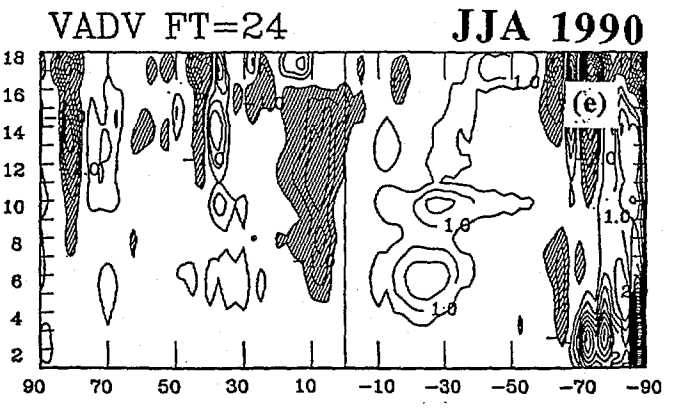
VADV FT=24
JJA 1990
(e)
18
16
14
12
10
8
6
4
2
90 70 50 30 10 -10 -30 -50 -70 -90

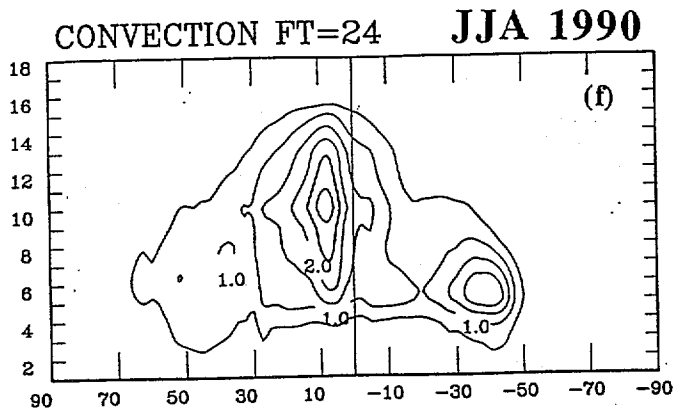
CONVECTION FT=24
JJA 1990
(f)
1.0
2.0
1.0
1.0
18 16 14 12 10 8 6 4 2
90 70 50 30 10 −10 −30 −50 −70 −90

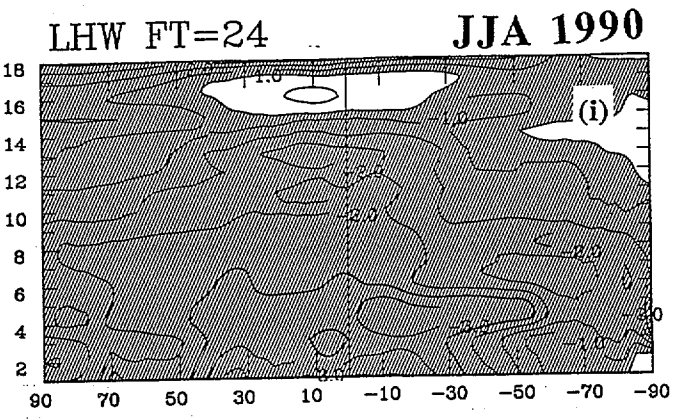
LHW FT=24
JJA 1990
(i)
18 16 14 12 10 8 6 4 2
90 70 50 30 10 −10 −30 −50 −70 −90

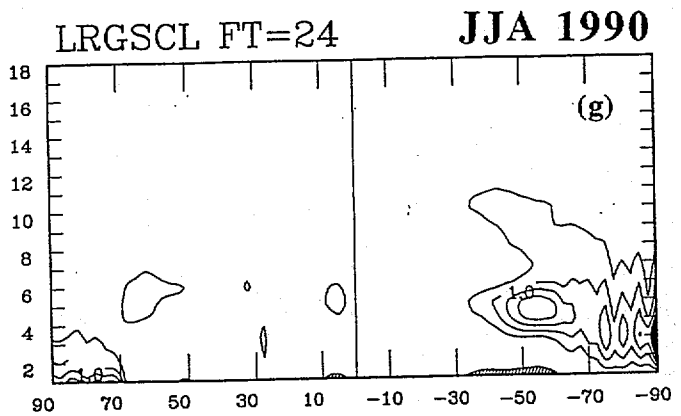
LRGSCL FT=24
JJA 1990
(g)
18 16 14 12 10 8 6 4 2
90 70 50 30 10 −10 −30 −50 −70 −90

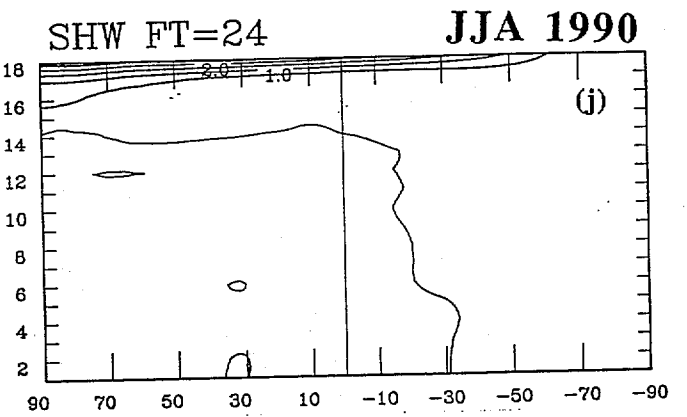
SHW FT=24
JJA 1990
(j)
2.0
1.0
18 16 14 12 10 8 6 4 2
90 70 50 30 10 −10 −30 −50 −70 −90

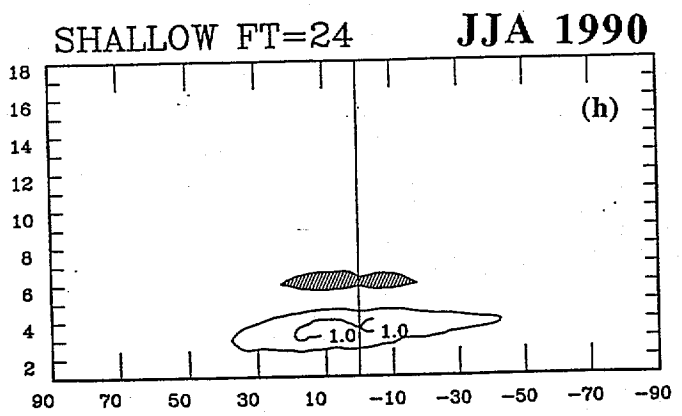
SHALLOW FT=24
JJA 1990
(h)
1.0
1.0
18 16 14 12 10 8 6 4 2
90 70 50 30 10 −10 −30 −50 −70 −90

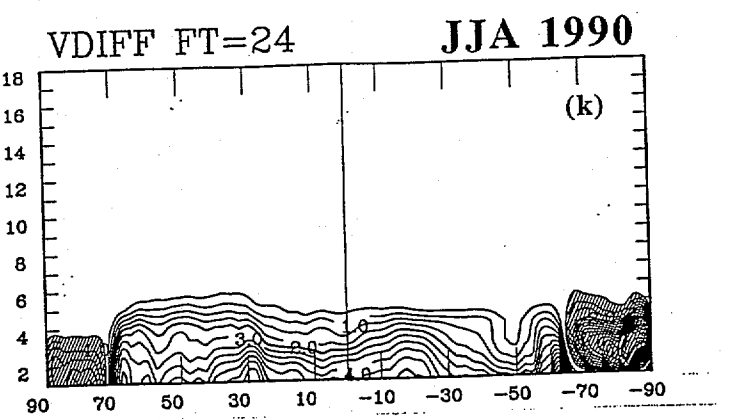
VDIFF FT=24
JJA 1990
(k)
18 16 14 12 10 8 6 4 2
90 70 50 30 10 −10 −30 −50 −70 −90

HEAT MODEL TENDENCY SIGMA 1 **JJA 1990**

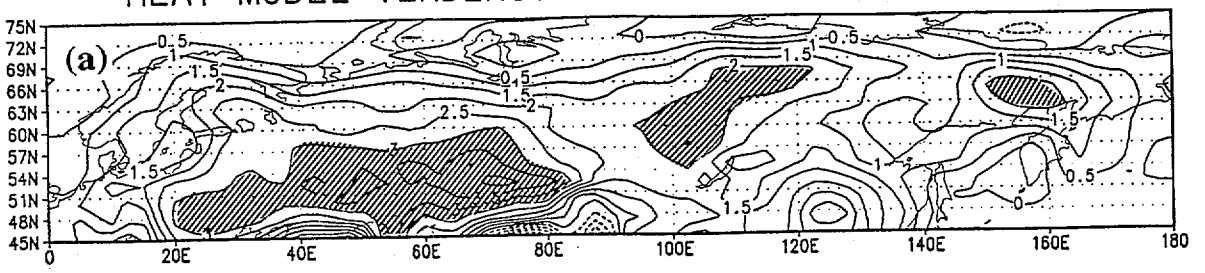

HEAT VPSIDELT SIGMA 1 **JJA 1990**

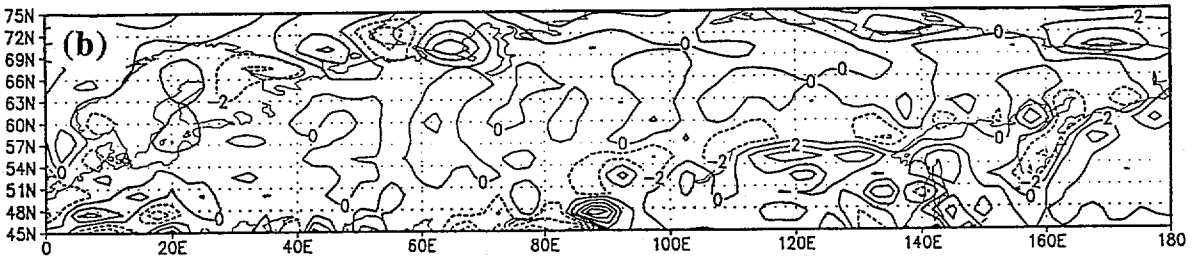

HEAT VCHIDELT SIGMA 1 **JJA 1990**

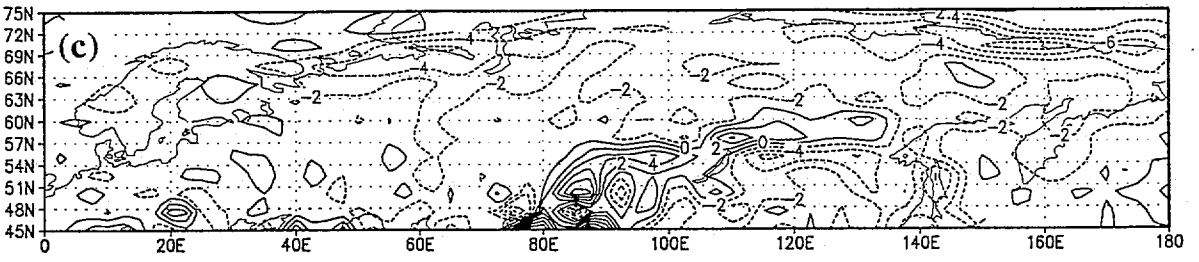

HEAT RTLNPS SIGMA 1 **JJA 1990**

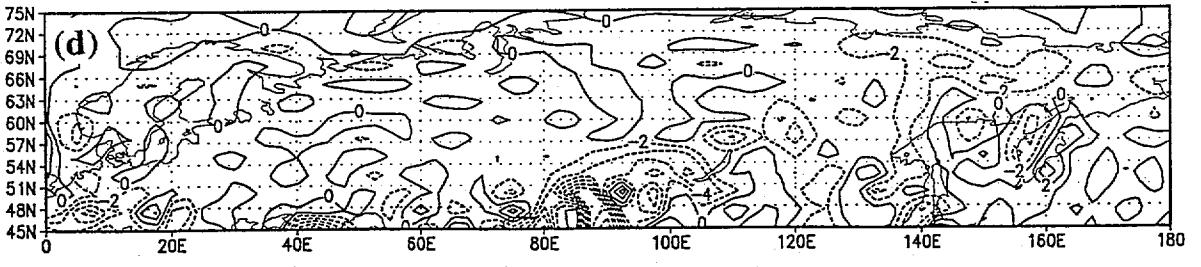

HEAT VERT DIFF SIGMA 1 **JJA 1990**

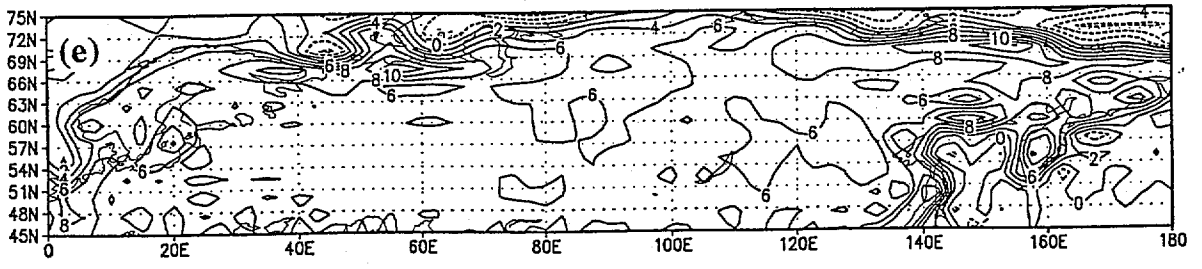

(RTLNPS+VCHIDELT+VPSIDELT+VDIFF) SIGMA 1 **JJA 1990**

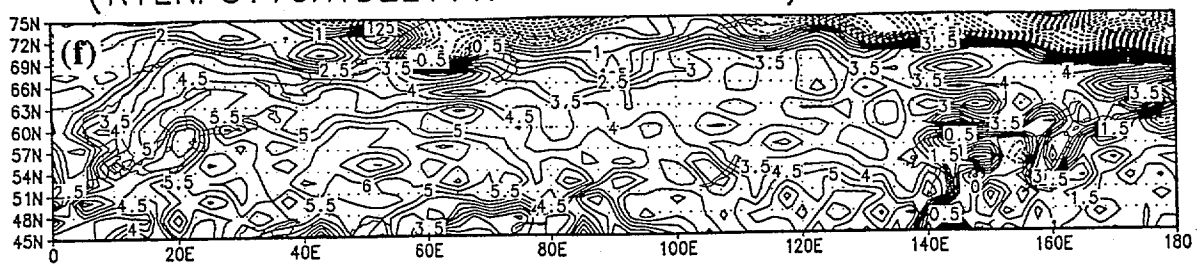

HEAT HORIZ DIFFUSION SIGMA 1 **JJA 1990**

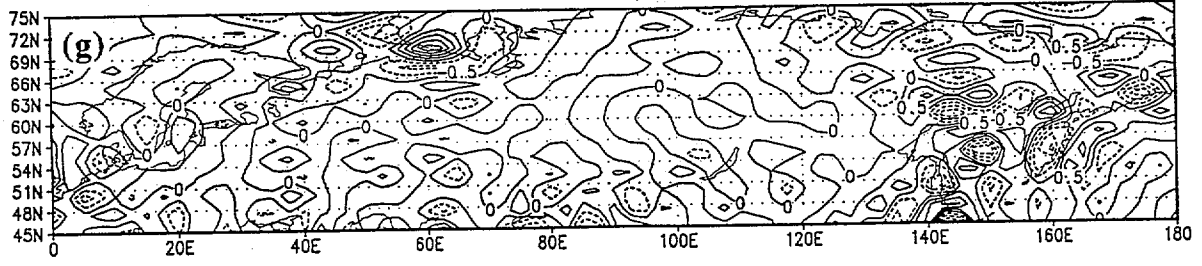

HEAT SUM EXCEPT LONGW SIGMA 1 **JJA 1990**

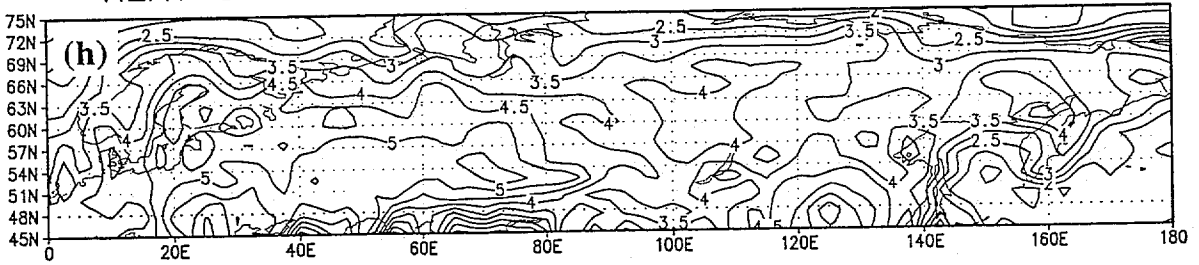

HEAT LONGWAVE SIGMA 1 **JJA 1990**

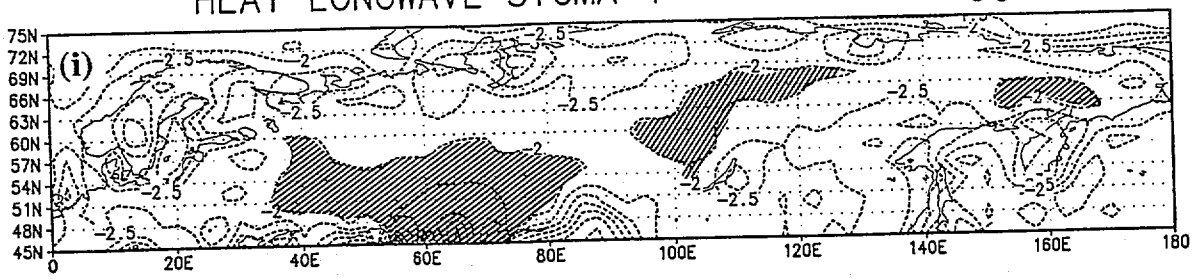

Temp Error Lev=1 S.H. Winter 1990

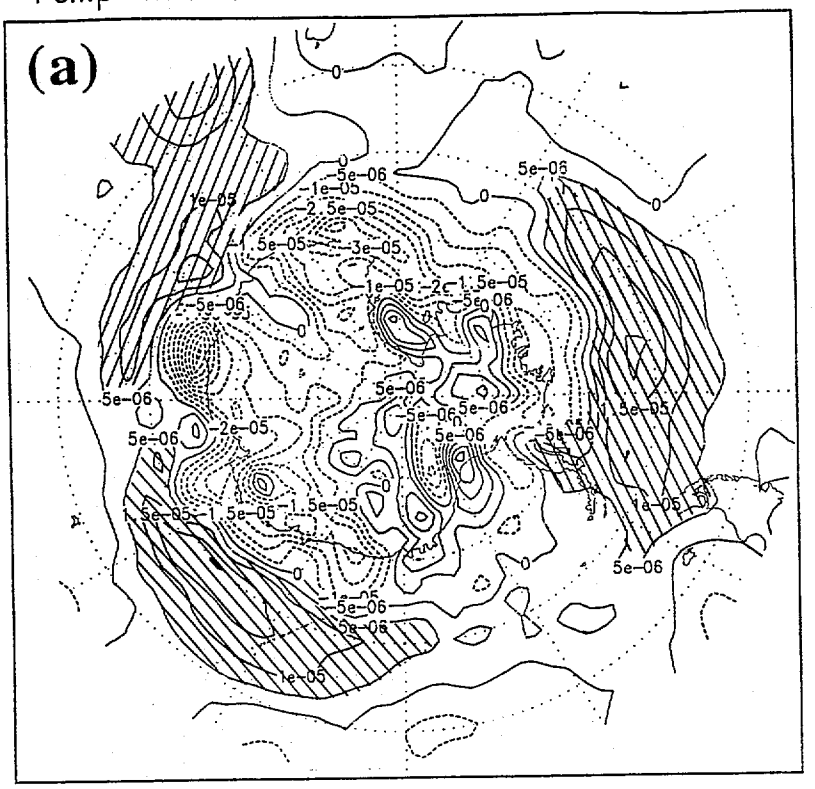

Temp Vdiff Lev=1 S.H. Winter 1990

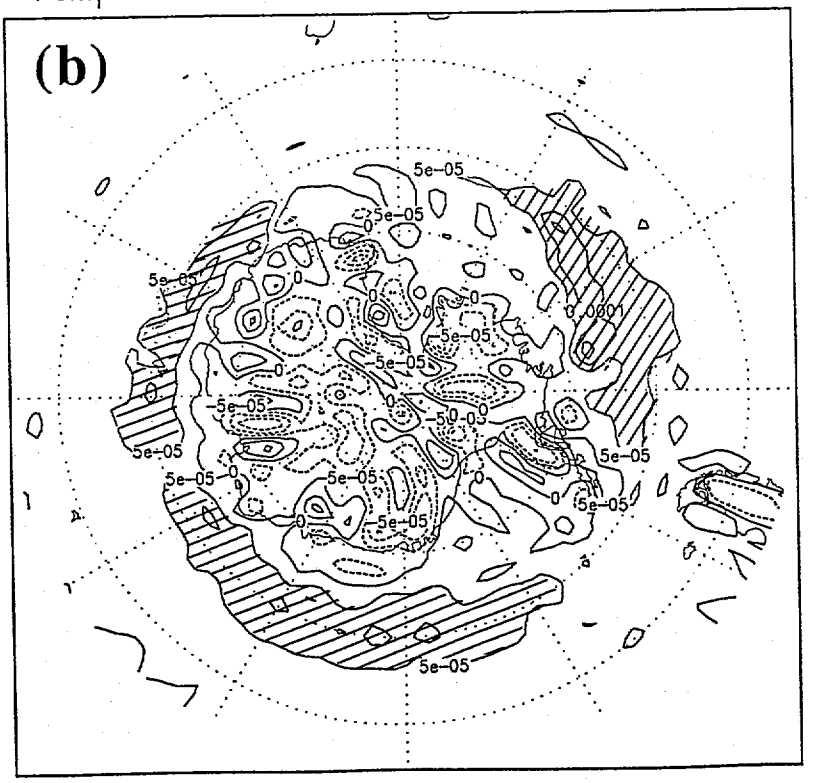

Fig 4

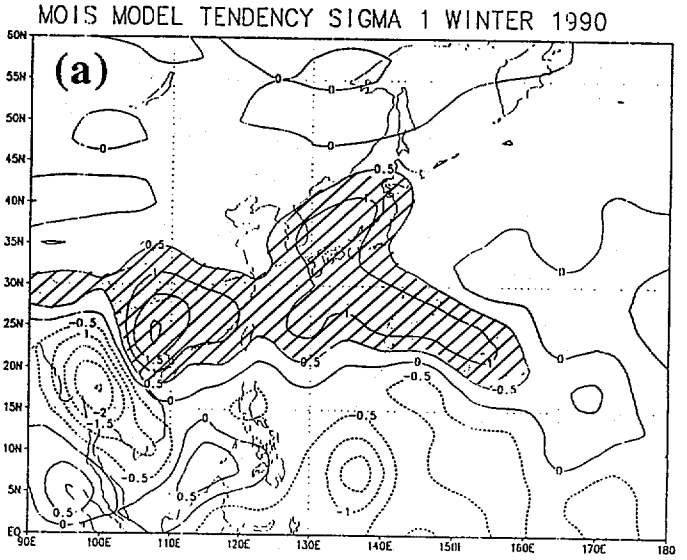
MOIS MODEL TENDENCY SIGMA 1 WINTER 1990
(a)
60N
55N
50N
45N
40N
35N
30N
25N
20N
15N
10N
5N
EQ
90E
100E
110E
120E
130E
140E
150E
160E
170E
180

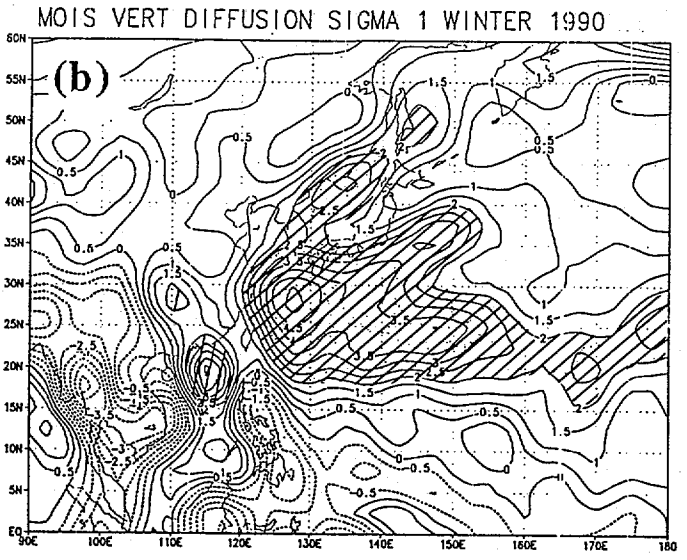
MOIS VERT DIFFUSION SIGMA 1 WINTER 1990
(b)
60N
55N
50N
45N
40N
35N
30N
25N
20N
15N
10N
5N
EQ
90E
100E
110E
120E
130E
140E
150E
160E
170E
180

Fig 5

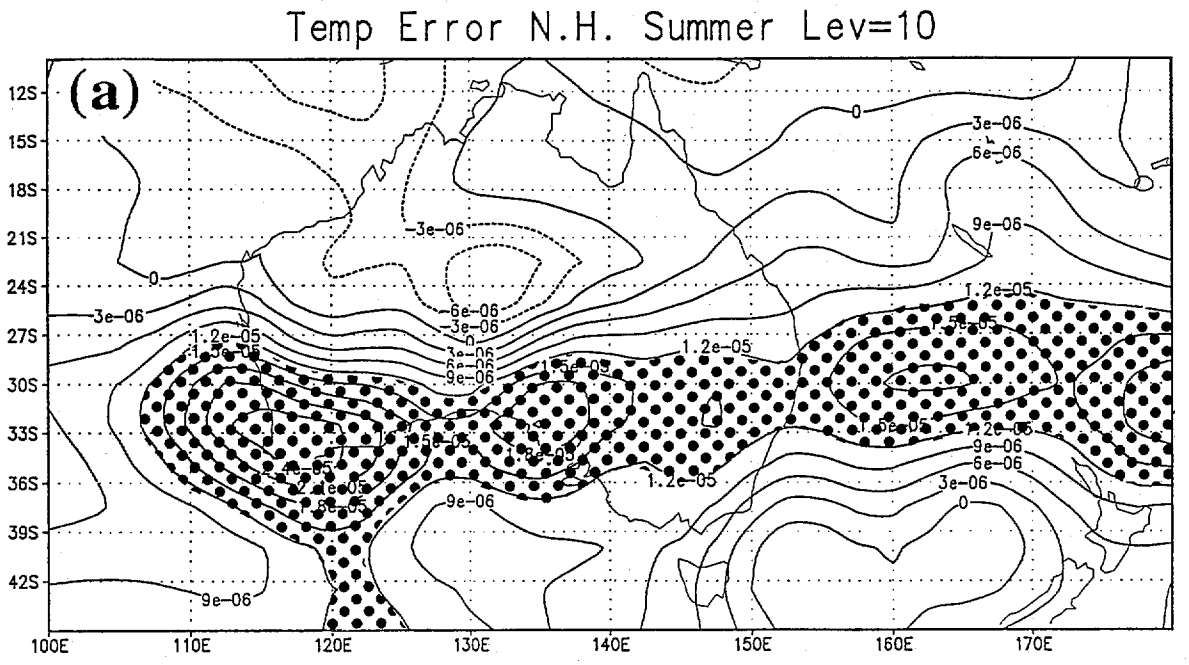
Temp Error N.H. Summer Lev=10
(a)
12S
15S
18S
21S
24S
27S
30S
33S
36S
39S
42S
100E
110E
120E
130E
140E
150E
160E
170E
-3e-06
0
3e-06
6e-06
9e-06
1.2e-05
-9e-06

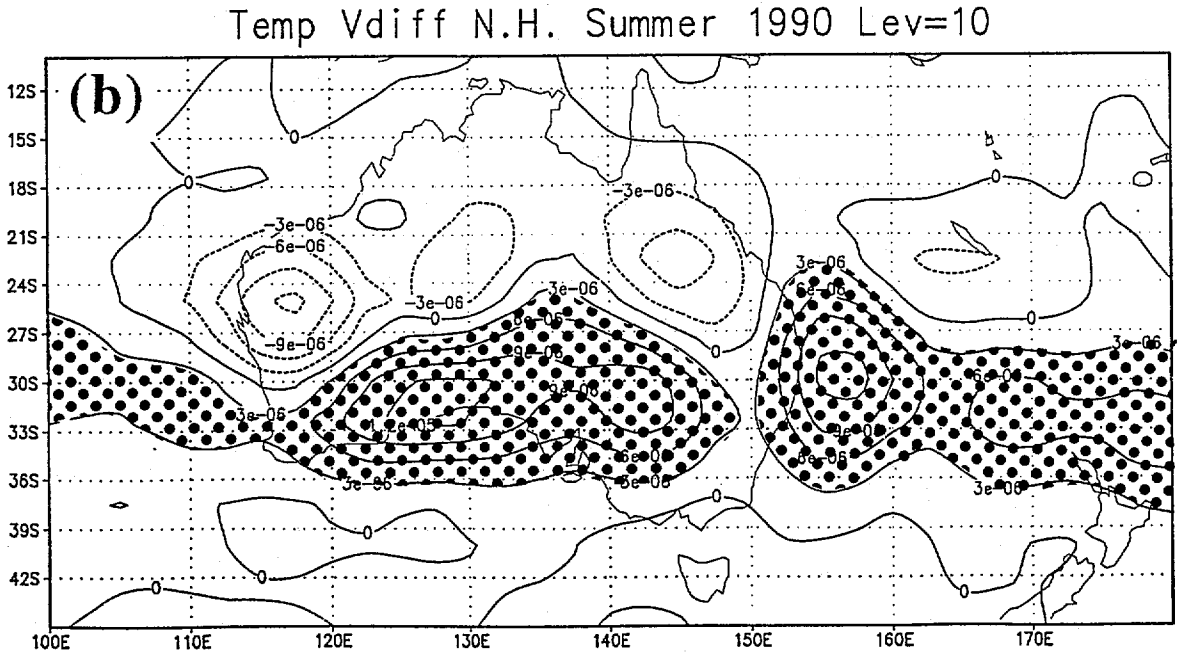
Temp Vdiff N.H. Summer 1990 Lev=10
(b)
12S
15S
18S
21S
24S
27S
30S
33S
36S
39S
42S
100E
110E
120E
130E
140E
150E
160E
170E
-3e-06
0
3e-06
6e-06
9e-06
-9e-06

Temp Error N.H. Winter 1990 Lev=10

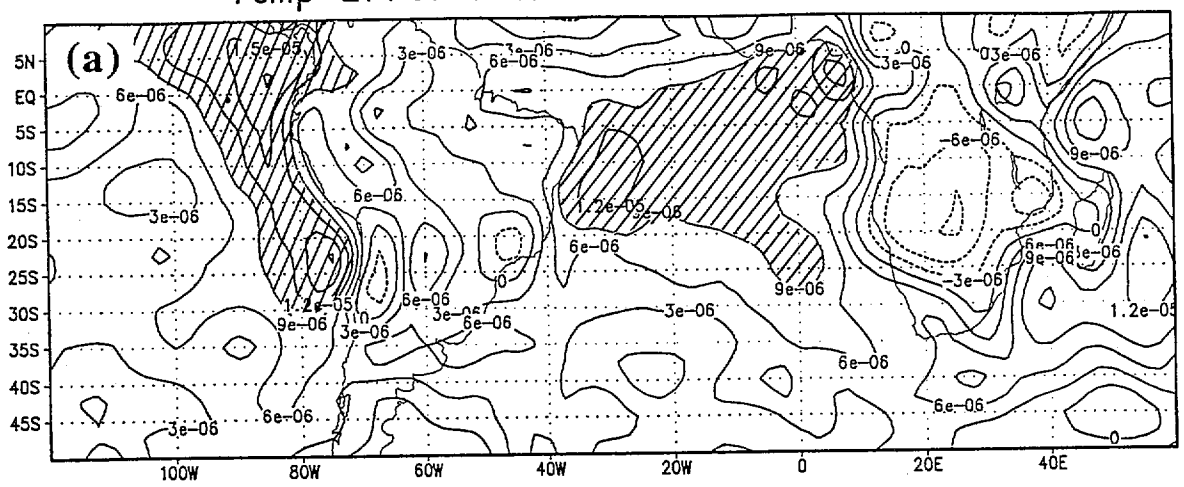

Temp Dynamics N.H. Winter 1990 Lev=10

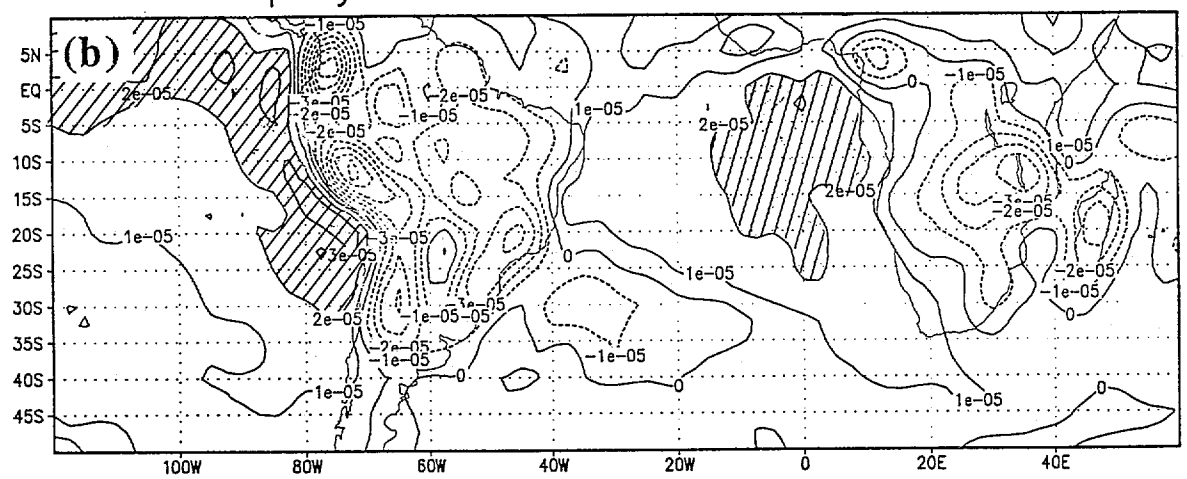

Temp Longwave N.H. Winter 1990 Lev=10

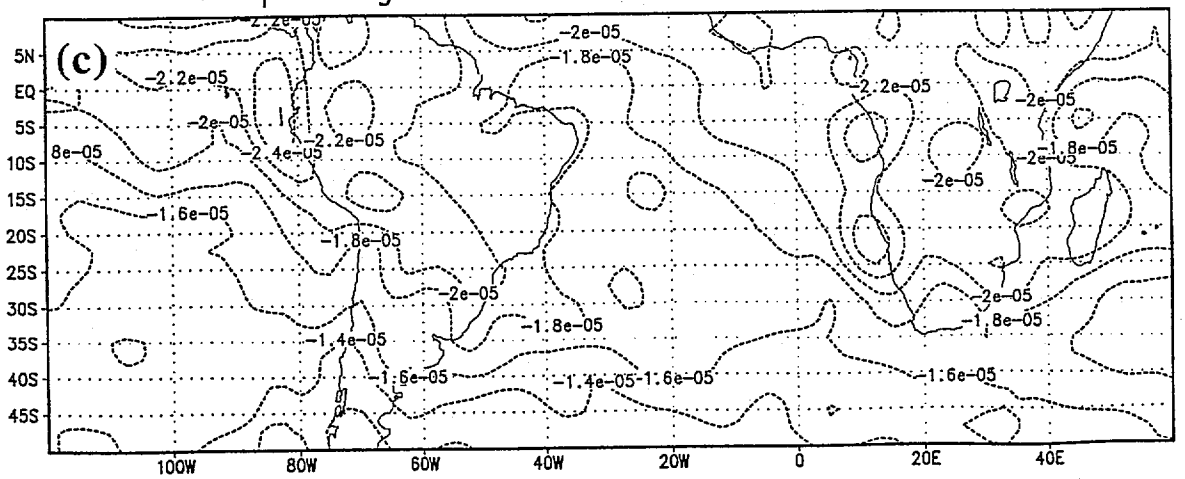

Temp Error N.H. Summer 1990 Lev=10

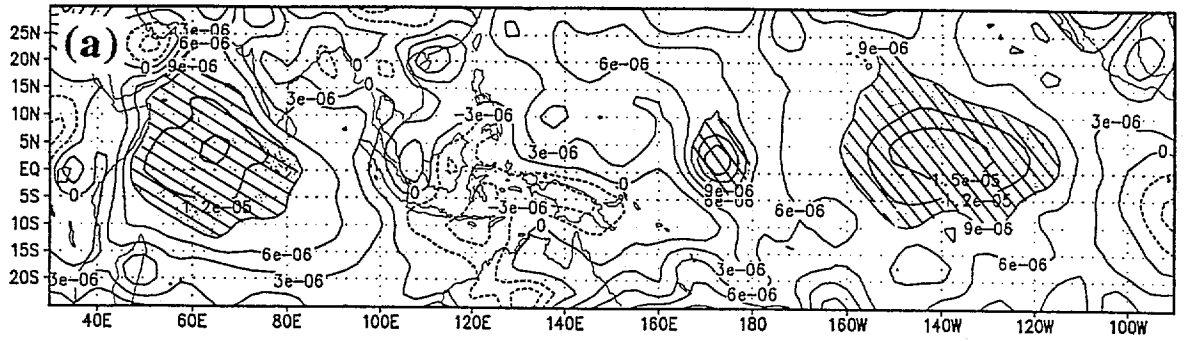

Temp Convection N.H. Summer 1990 Lev=10

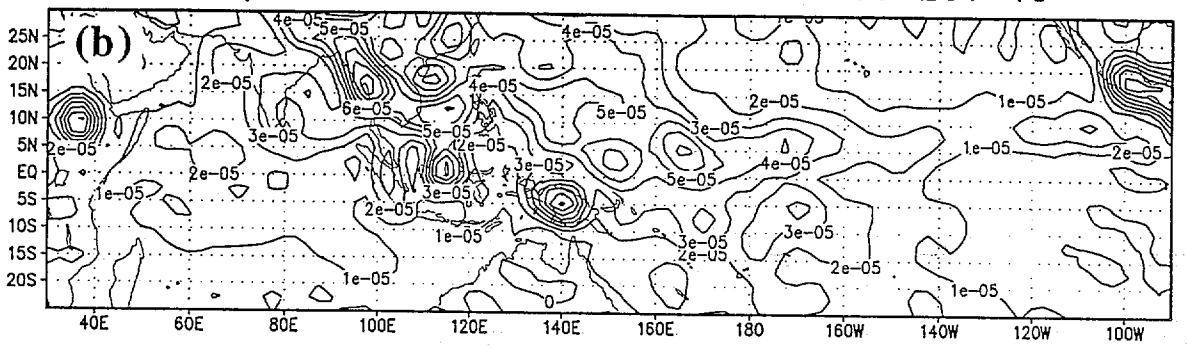

Temp Longwave N.H. Summer 1990 Lev=10

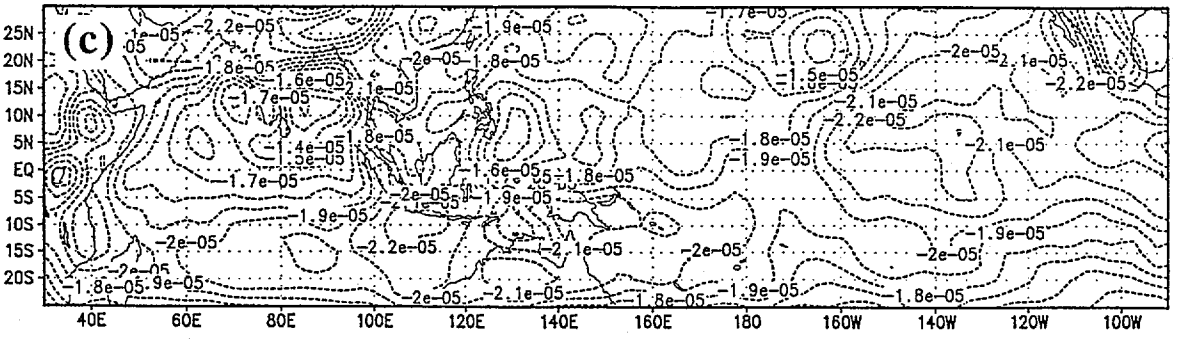

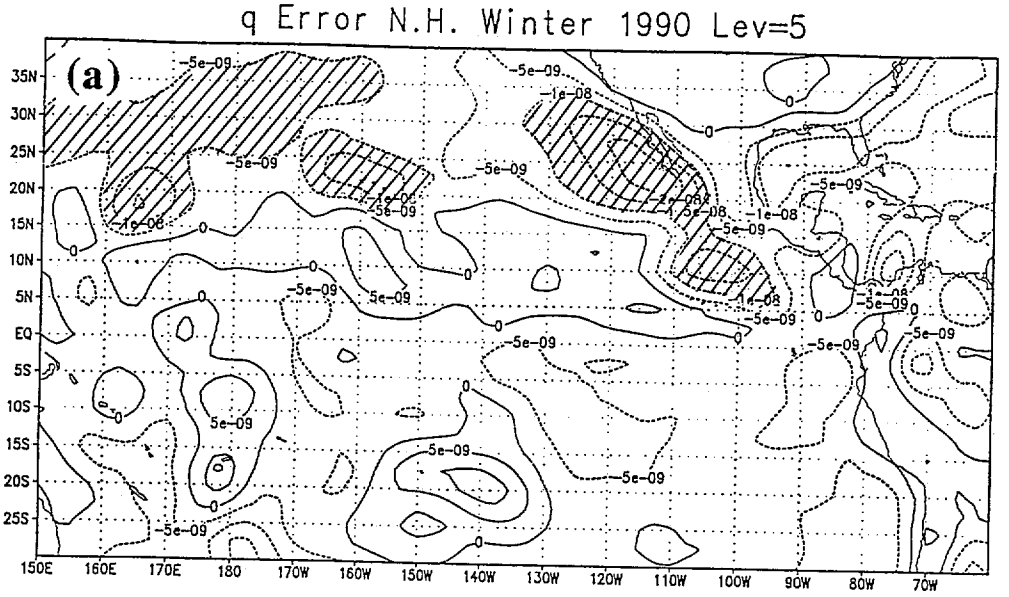
q Error N.H. Winter 1990 Lev=5
(a)
35N
30N
25N
20N
15N
10N
5N
EQ
5S
10S
15S
20S
25S
150E
160E
170E
180
170W
160W
150W
140W
130W
120W
110W
100W
90W
80W
70W

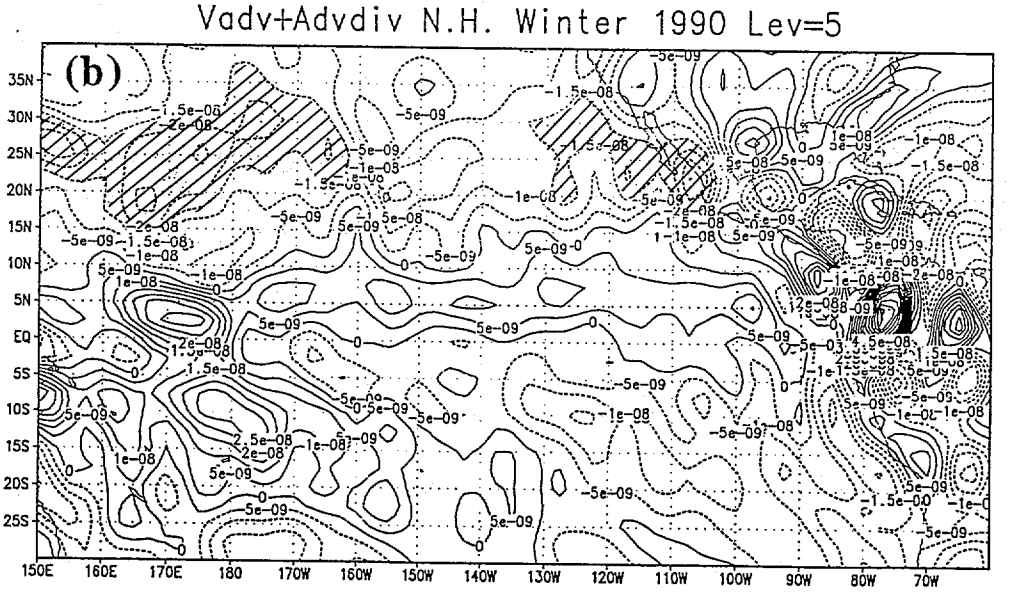
Vadv+Advdiv N.H. Winter 1990 Lev=5
(b)
35N
30N
25N
20N
15N
10N
5N
EQ
5S
10S
15S
20S
25S
150E
160E
170E
180
170W
160W
150W
140W
130W
120W
110W
100W
90W
80W
70W

q Convection N.H. Winter 1990 Lev=5

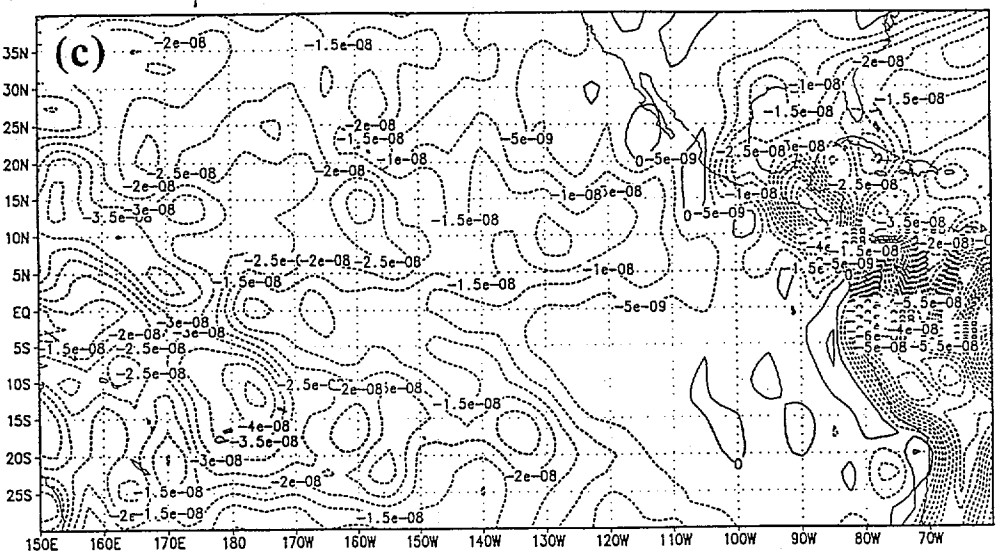

q Vdiff N.H. Winter 1990 Lev=5

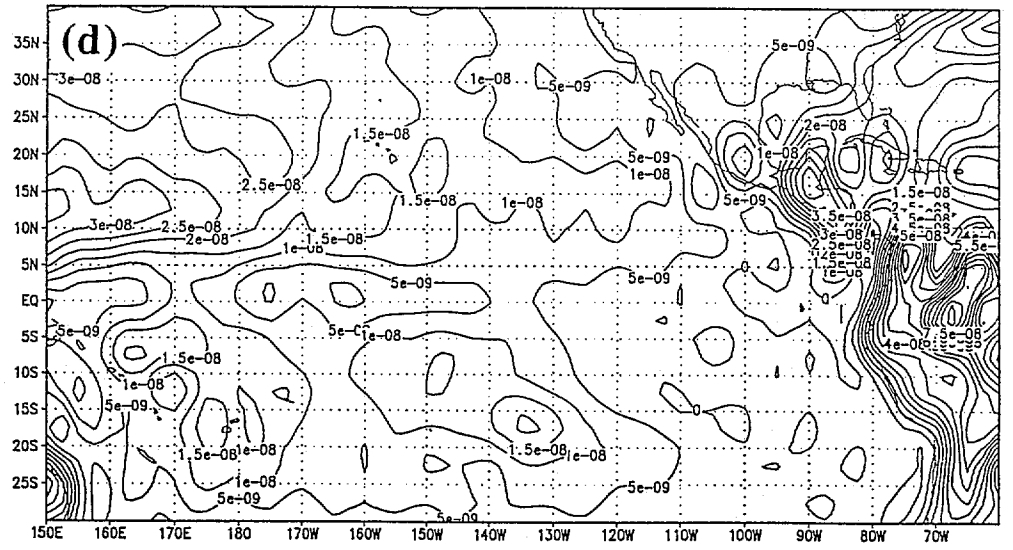

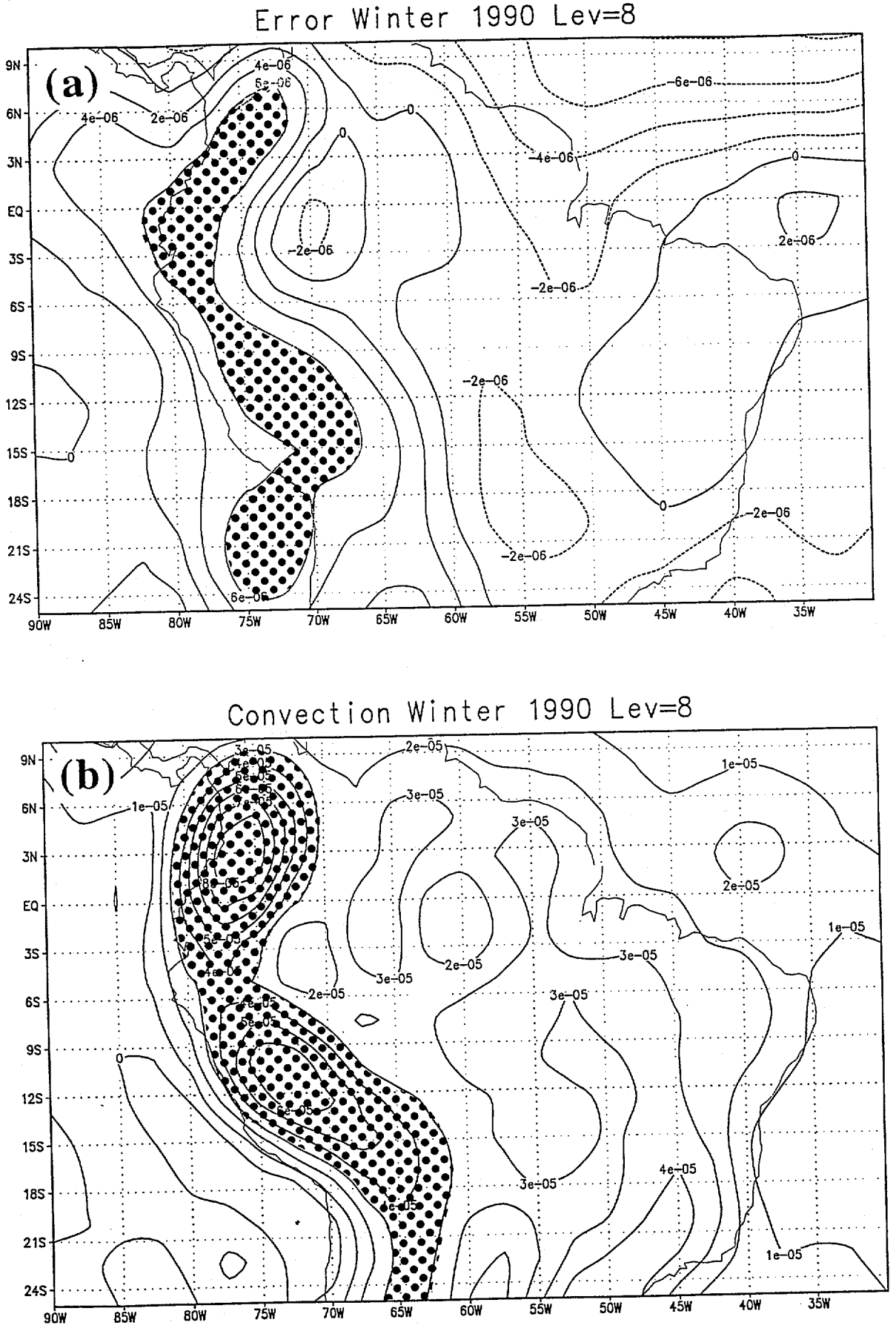
Error Winter 1990 Lev=8
(a)
Convection Winter 1990 Lev=8
(b)
9N
6N
3N
EQ
3S
6S
9S
12S
15S
18S
21S
24S
90W
85W
80W
75W
70W
65W
60W
55W
50W
45W
40W
35W

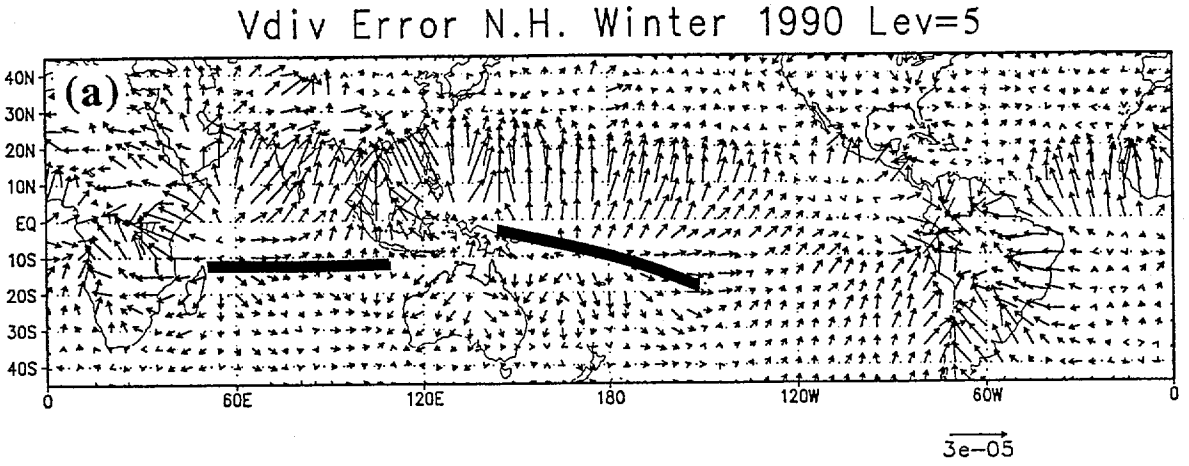
Vdiv Error N.H. Winter 1990 Lev=5
(a)
40N
30N
20N
10N
EQ
10S
20S
30S
40S
0
60E
120E
180
120W
60W
0
3e-05

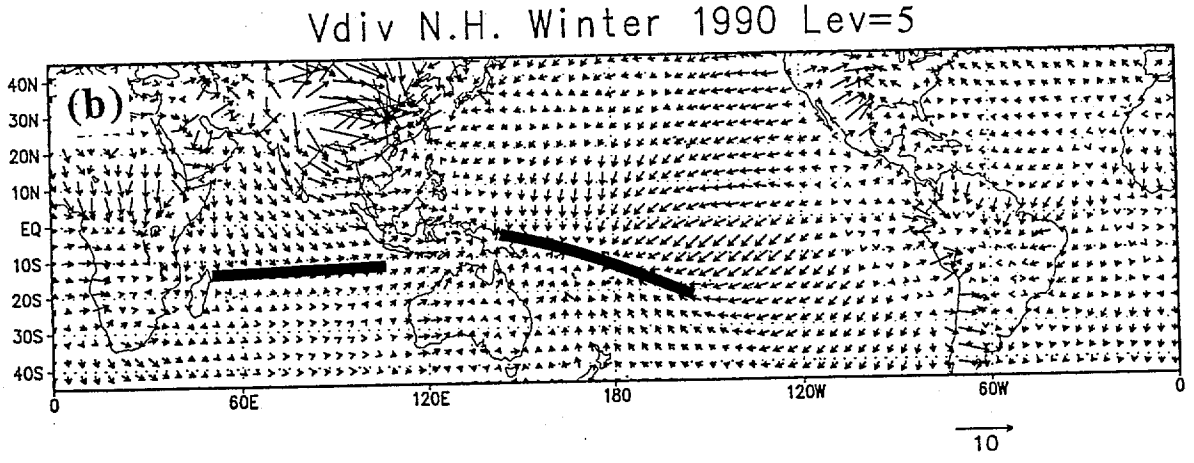
Vdiv N.H. Winter 1990 Lev=5
(b)
40N
30N
20N
10N
EQ
10S
20S
30S
40S
0
60E
120E
180
120W
60W
0
10

Temp Error Winter 1990 Lev=17

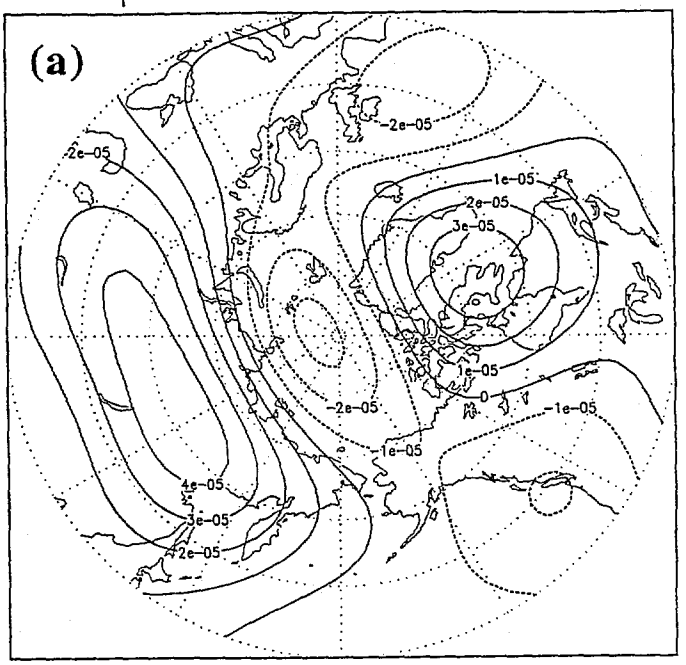

Temp Advrot Winter 1990 Lev=17

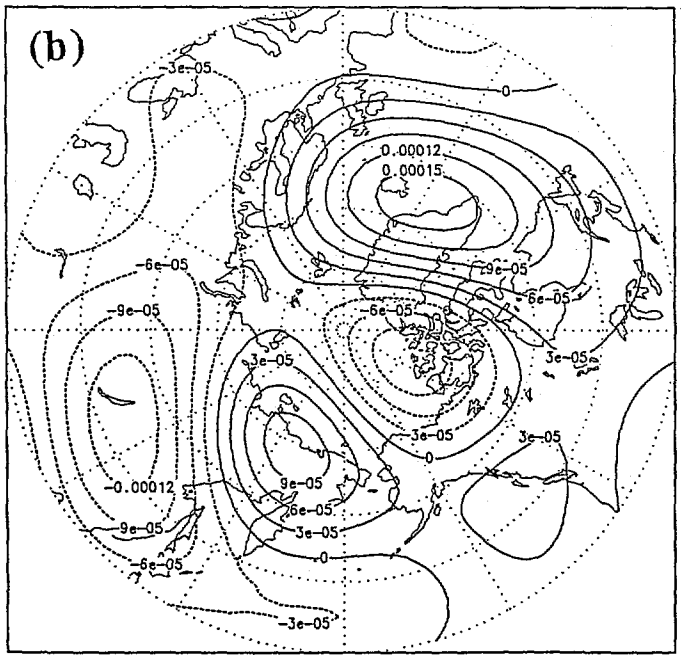

Temp Advdiv+Lnps+Vadv Winter 1990 Lev=17

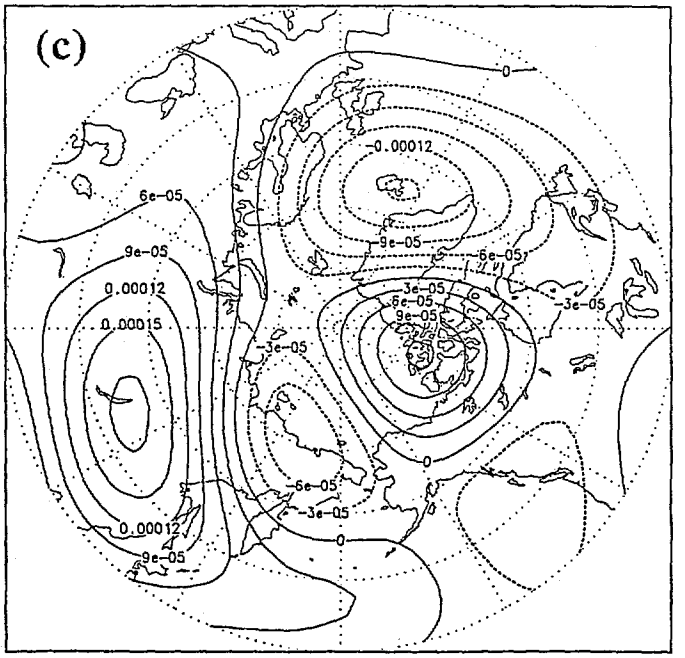

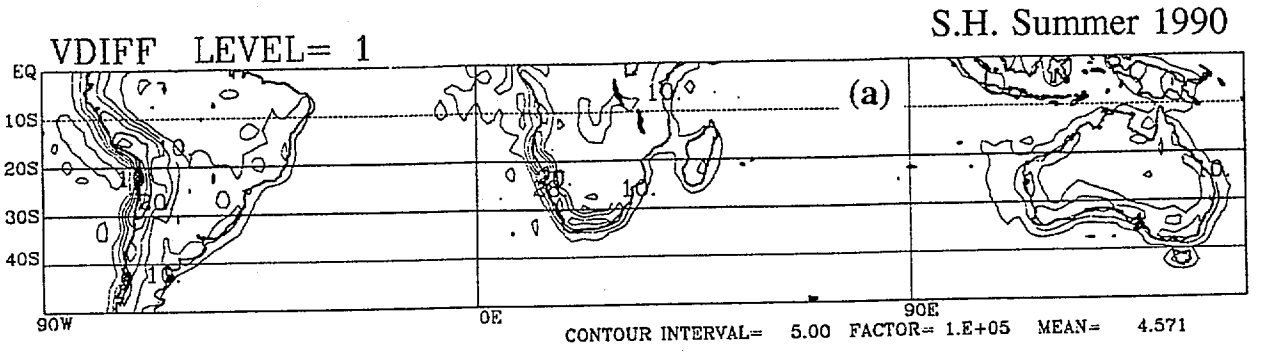
S.H. Summer 1990
VDIFF LEVEL= 1
(a)
EQ
10S
20S
30S
40S
90W
0E
90E
CONTOUR INTERVAL= 5.00 FACTOR= 1.E+05 MEAN= 4.571

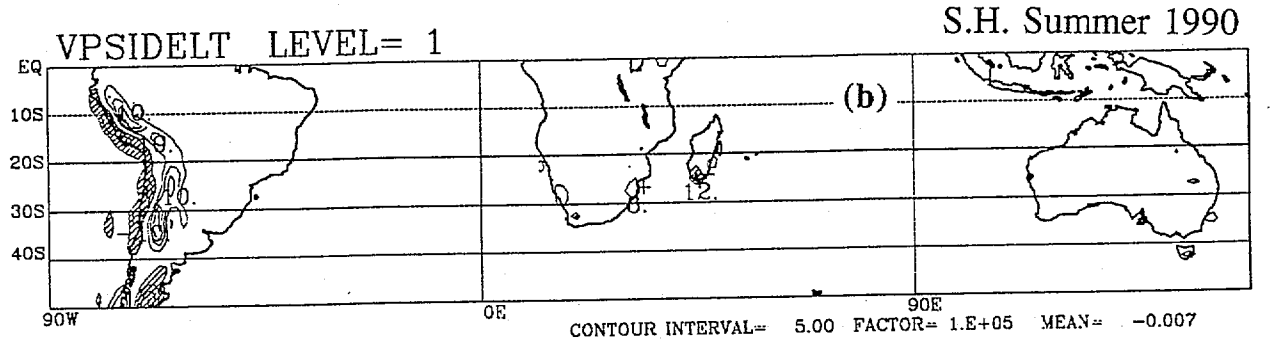
S.H. Summer 1990
VPSIDELT LEVEL= 1
(b)
EQ
10S
20S
30S
40S
90W
0E
90E
CONTOUR INTERVAL= 5.00 FACTOR= 1.E+05 MEAN= -0.007

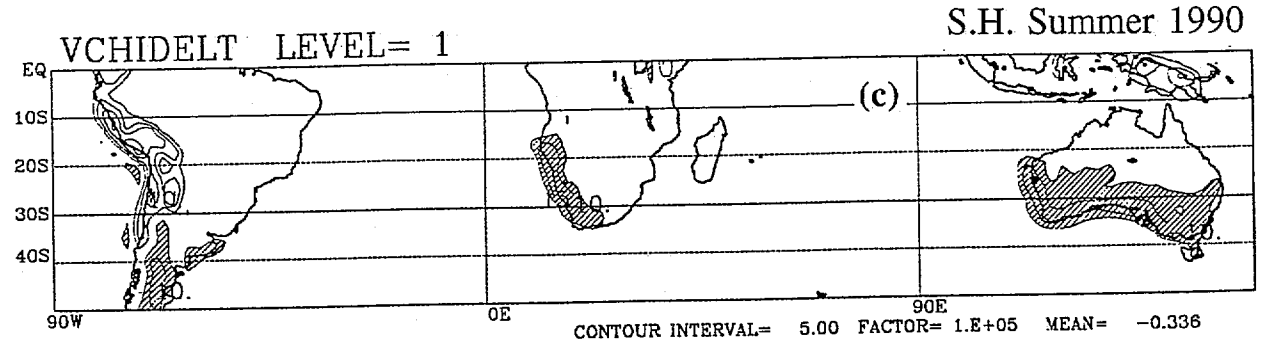
S.H. Summer 1990
VCHIDELT LEVEL= 1
(c)
EQ
10S
20S
30S
40S
90W
0E
90E
CONTOUR INTERVAL= 5.00 FACTOR= 1.E+05 MEAN= -0.336

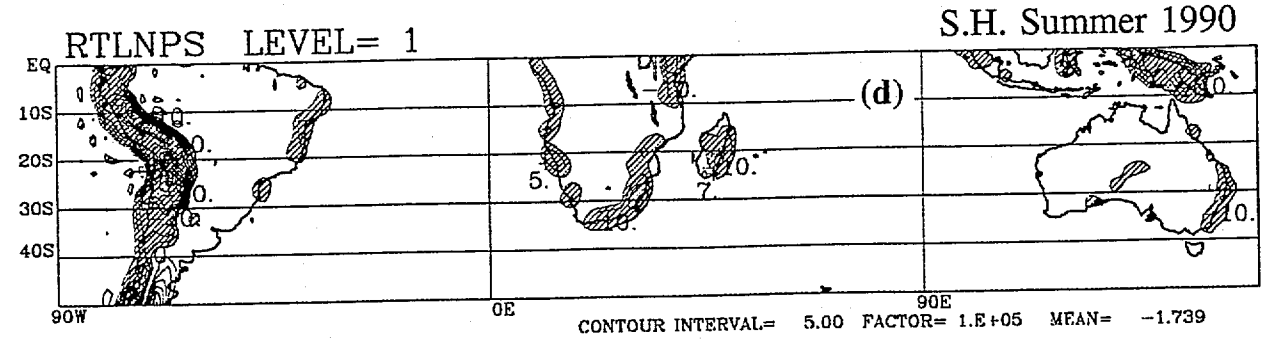
S.H. Summer 1990
RTLNPS LEVEL= 1
(d)
EQ
10S
20S
30S
40S
90W
0E
90E
CONTOUR INTERVAL= 5.00 FACTOR= 1.E+05 MEAN= -1.739

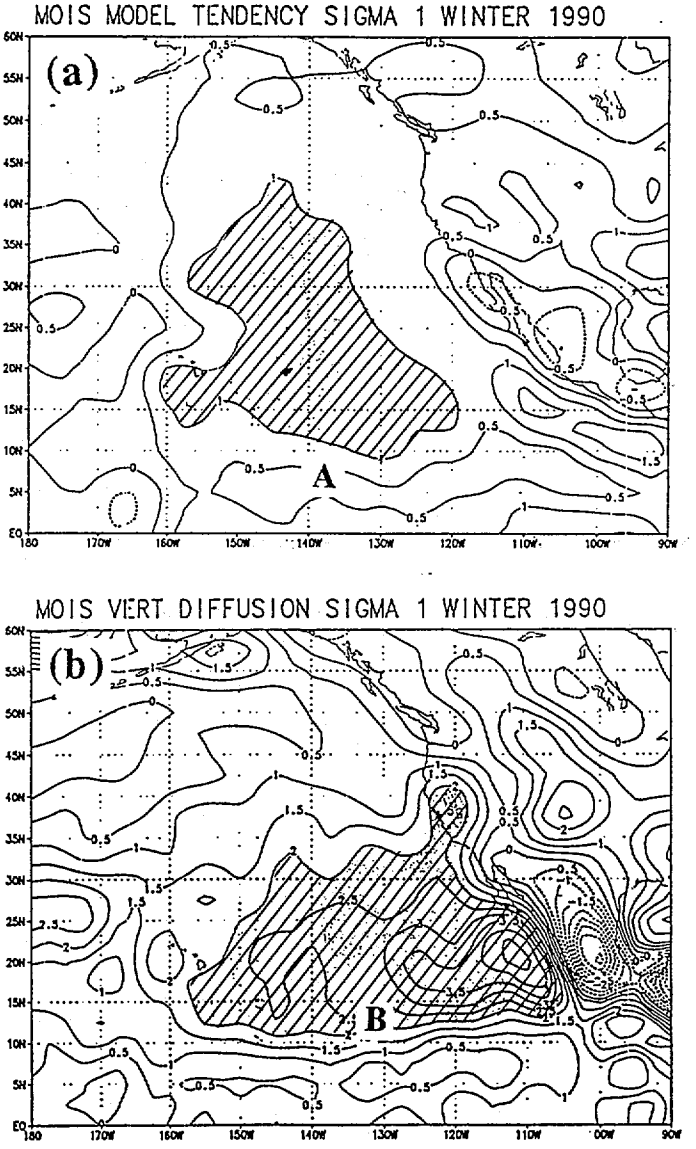
MOIS MODEL TENDENCY SIGMA 1 WINTER 1990
(a)
A
MOIS VERT DIFFUSION SIGMA 1 WINTER 1990
(b)
B

Fig 14

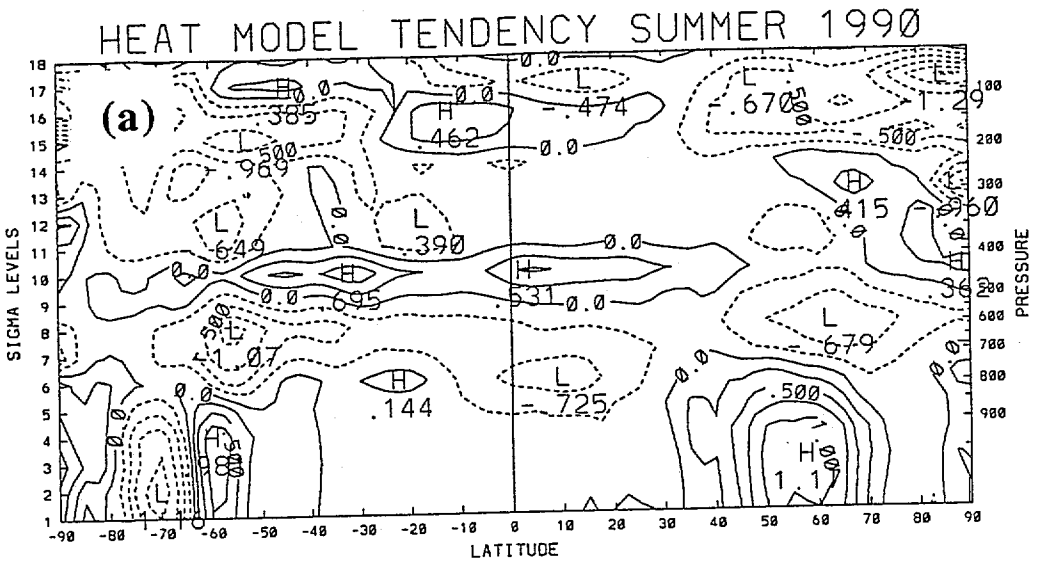
HEAT MODEL TENDENCY SUMMER 1990
(a)
SIGMA LEVELS
PRESSURE
LATITUDE

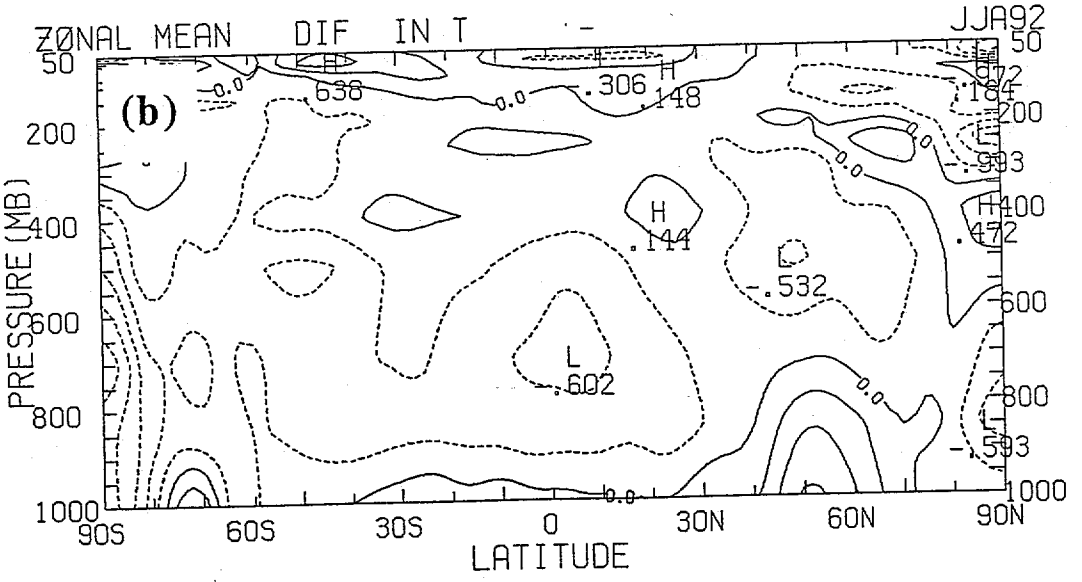
ZONAL MEAN DIF IN T
JJA92
(b)
PRESSURE (MB)
LATITUDE

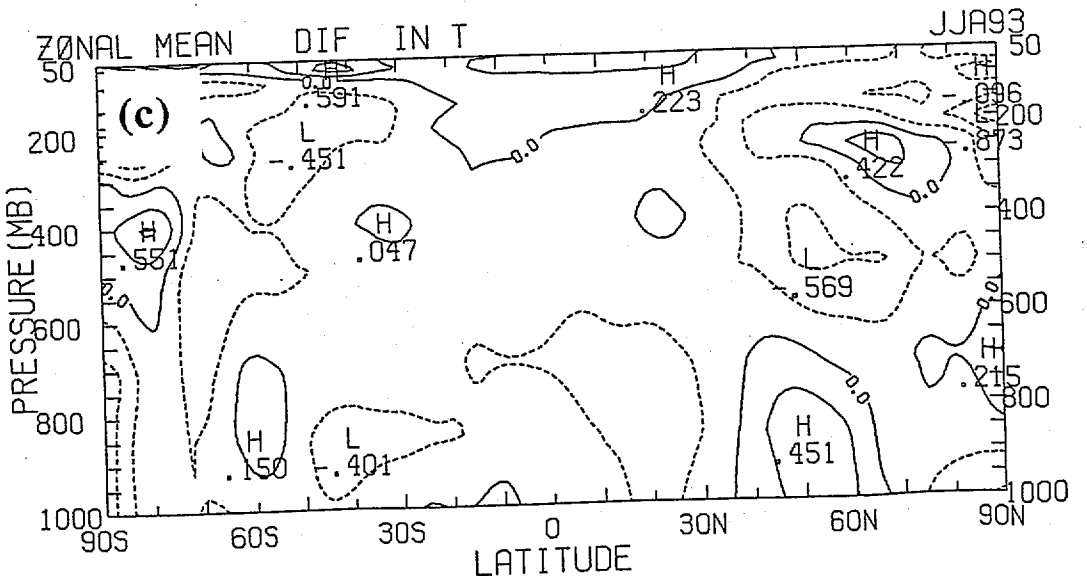
ZONAL MEAN DIF IN T
JJA93
(c)
PRESSURE (MB)
LATITUDE